16

Measurement and Characterization of Solar Cells and Modules

Keith Emery

National Renewable Energy Laboratory, Golden, CO, USA

16.1 INTRODUCTION

Methods of assessing the performance of photovoltaic cells and modules are described in this chapter. The performance of cells and modules can be described by their current versus voltage ($I-V$) and spectral responsivity versus wavelength ($S(\lambda)$) characteristics. Measurement equipment, procedures, and artifacts are discussed for $I-V$ and $S(\lambda)$. The most common performance indicator is the photovoltaic (PV) efficiency under standard reporting conditions (SRC) (temperature, spectral irradiance, total irradiance). The efficiency is the maximum electrical power divided by the total irradiance. Procedures for accurately determining the efficiency or the maximum power with respect to reference conditions are described. Alternatives to the standard peak watt rating and how they compare with actual field performance are discussed. Since photovoltaics must operate for 20 to 30 years, with a degradation of less than 1% per year, procedures for assessing the durability of PV modules are also discussed.

16.2 RATING PV PERFORMANCE

A variety of performance indicators have been employed by the photovoltaic community to rate the performance of PV cells and modules [1–4]. Domestic and international consensus standards have been adopted to rate the performance of PV cells and modules in terms of the output power, or equivalently their efficiency with respect to SRC defined by temperature, spectral irradiance, and total irradiance [5–15]. Modules and systems are rated by their peak power under SRC because manufacturers sell and customers purchase PV modules and systems according to the price per watt of power produced. Other performance indicators may be more appropriate for niche markets, such as aesthetics

Handbook of Photovoltaic Science and Engineering. Edited by A. Luque and S. Hegedus
 ISBN: 0-471-49196-9

for building-integrated photovoltaics, liters per day for water pumping, or low light-level operation for consumer electronics [4].

The actual output of a PV module or system in the field is a function of orientation, total irradiance, spectral irradiance, wind speed, air temperature, soiling, and various system-related losses. Various module- and system-rating methods attempt to ensure that the actual performance is comparable to the rated performance to keep the resulting level of customer satisfaction high.

16.2.1 Standard Reporting Conditions

The PV performance in terms of SRC is commonly expressed in terms of efficiency. At the research level, an internationally accepted set of SRC is essential to prevent the researcher from adjusting the reporting conditions to maximize the efficiency. The procedures for measuring the performance with respect to SRC must be quick, easy, reproducible, and accurate for the research cell fresh out of the deposition system or for the module on a factory floor with production goals. The PV conversion efficiency (η) is calculated from the measured maximum or peak PV power (P_{max}), device area (A), and total incident irradiance (E_{tot}):

$$\eta = \frac{P_{max}}{E_{tot}A}100 \tag{16.1}$$

The term *reporting*, rather than *reference* or *test*, is used because a measurement can be performed at conditions other than SRC and then carefully corrected to be equivalent to being measured at SRC. The SRC for rating the performance of cells and modules are summarized in Table 16.1 [1, 5–15]. The direct, global, and AM0 reference spectra are summarized in Figure 16.1 and Tables 16.2 and 16.3.

As a matter of shorthand, the global and direct terrestrial reference spectra are often referred to as AM1.5 G and AM1.5 D, respectively. Many groups often just refer to the reference spectrum as AM1.5. This can be confusing without a reference because numerous different AM1.5 reference spectra have been proposed and used in the past. It should be noted that neither the direct reference spectrum nor the global reference spectrum actually integrates to exactly 1000 Wm^{-2} [10, 12, 13, 17]. The global reference spectrum integrates to approximately 963 Wm^{-2} and the direct reference spectrum

Table 16.1 Standard reference conditions for rating photovoltaic cells, modules and systems

Application	Irradiance [Wm^{-2}]	Reference Spectrum	Temperature [°C]
Terrestrial			
Cells	1000	Global [5]	25 cell [5, 6, 11]
Modules, systems	1000	Global [11, 13]	25 cell [7] or NOCT [7]
Modules, systems	1000[a]	Prevailing	20 ambient
Concentration[b]	>1000	Direct [10]	25 cell [5]
Extraterrestrial[c]	1366 [8], 1367 [14]	AM0 [8, 14, 15]	25 [15], 28 cell [16]

[a] Linear regression of power to project test conditions, 850 Wm^{-2} with a 5° field of view for concentrator systems
[b] At present, no consensus standards exist although ASTM and the European Community are developing standards
[c] At present no consensus standards exist although there is an ISO draft standard [15]

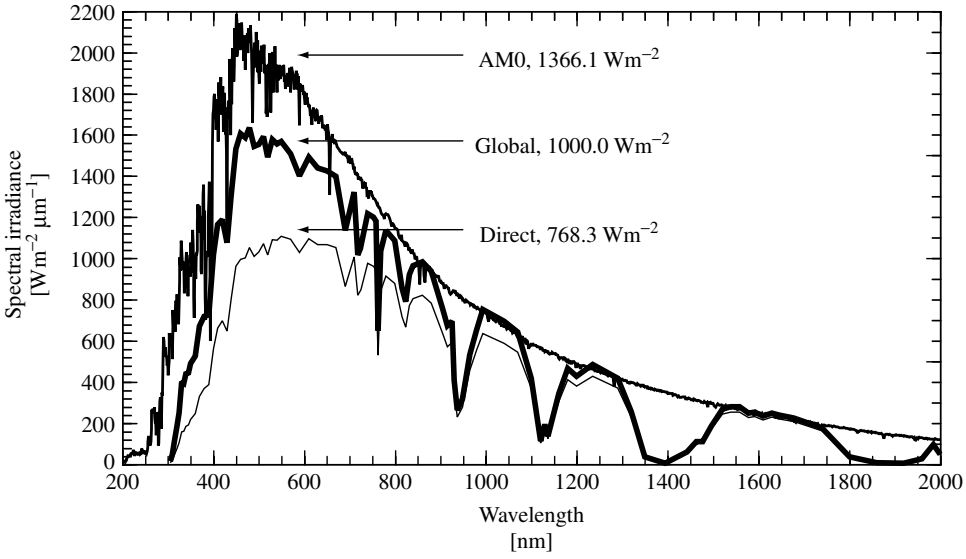

Figure 16.1 Global, Direct, and AM0 reference spectra listed in Tables 16.2 and 16.3. Adapted with permission from the Annual Book of ASTM Standards, Copyright ASTM [10, 12, 13]

integrates to approximately 768 Wm^{-2}. Different numerical integration methods give differences in the integrated or total irradiance of the reference spectra at the 0.1% level because of the relatively small number of data points (120) and the large variations in the spectral irradiance with wavelength. The structure in the spectral irradiance is a function of bandwidth. The bandwidth in the spectral irradiance at any given wavelength is approximately the difference in wavelength between adjacent points. The PV community has arbitrarily taken the term "one sun" to mean a total irradiance of 1000 Wm^{-2} [17]. In fact, the spectral irradiance of the global reference spectrum normalized to 1000 Wm^{-2} in Table 16.2 and Figure 16.1 exceeds the AM0 spectral irradiance in the infrared, which is not physically possible without concentration. The term *global* in Tables 16.1 and 16.2 refers to the spectral irradiance distribution on a 37° tilted south-facing surface with a solar zenith angle of 48.19° (AM1.5). The term *direct* in Tables 16.1 and 16.2 refers to the direct-normal component (5° field of view) of the global spectral irradiance distribution [18]. The term AM1 or AM1.5 is often used to refer to standard spectra, but the relative optical air mass (AM) is a geometrical quantity and can be obtained by taking the secant of the zenith angle (See Section 20.3 for a more complete explanation of AM.). For AM1, the zenith angle is 0°. The relative optical air mass can be pressure-corrected to an absolute air mass by multiplying by the barometric pressure and dividing by the sea level pressure. In outer space the pressure is zero so the absolute air mass is always zero. The internationally accepted global reference spectrum is based upon the 1962 US standard atmosphere with a rural aerosol distribution as input to a sophisticated Monte Carlo ray-tracing model for wavelengths up to 2500 nm and an undocumented simple direct-normal spectral model for the irradiances from 2500 nm to 4050 nm [12, 13, 18]. The fact that the reference spectrum only approximates the "real-world" spectra at solar noon is unimportant as long as the differences between the photocurrents are the same for various PV

Table 16.2 Standard direct and global reference spectra adapted with permission from the annual book of ASTM standards, Copyright ASTM [10, 11]. The global spectrum integrates to 1000.0 Wm^{-2} and the direct spectrum integrates to 768.3 Wm^{-2}

Wavelength [nm]	Global [Wm^{-2} μm^{-1}]	Direct [Wm^{-2} μm^{-1}]	Wavelength [nm]	Global [Wm^{-2} μm^{-1}]	Direct [Wm^{-2} μm^{-1}]	Wavelength [nm]	Global [Wm^{-2} μm^{-1}]	Direct [Wm^{-2} μm^{-1}]
–	–	–	–	–	–	–	–	–
305	9.5	3.4	740	1211.2	971.0	1520	262.6	239.3
310	42.3	15.6	753	1193.9	956.3	1539	274.2	248.8
315	107.8	41.1	758	1175.5	942.2	1558	275.0	249.3
320	181.0	71.2	763	643.1	524.8	1578	244.6	222.3
325	246.8	100.2	768	1030.7	830.7	1592	247.4	227.3
330	395.3	152.4	780	1131.1	908.9	1610	228.7	210.5
335	390.1	155.6	800	1081.6	873.4	1630	244.5	224.7
340	435.3	179.4	816	849.2	712.0	1646	234.8	215.9
345	438.9	186.7	824	785.0	660.2	1678	220.5	202.8
350	483.7	212.0	832	916.4	765.5	1740	171.5	158.2
360	520.3	240.5	840	959.9	799.8	1800	30.7	28.6
370	666.2	324.0	860	978.9	815.2	1860	2.0	1.8
380	712.5	362.4	880	933.2	778.3	1920	1.2	1.1
390	720.7	381.7	905	748.5	630.4	1960	21.2	19.7
400	1013.1	556.0	915	667.5	565.2	1985	91.1	84.9
410	1158.2	656.3	925	690.3	586.4	2005	26.8	25.0
420	1184.0	690.8	930	403.6	348.1	2035	99.5	92.5
430	1071.9	641.9	937	258.3	224.2	2065	60.4	56.3
440	1302.0	798.5	948	313.6	271.4	2100	89.1	82.7
450	1526.0	956.6	965	526.8	451.2	2148	82.2	76.2
460	1599.6	990.8	980	646.4	549.7	2198	71.5	66.4
470	1581.0	998.0	993	746.8	630.1	2270	70.2	65.0
480	1628.3	1046.1	1040	690.5	582.9	2360	62.0	57.6
490	1539.2	1005.1	1070	637.5	539.7	2450	21.2	19.8
500	1548.7	1026.7	1100	412.6	366.2	2494	18.5	17.0
510	1586.5	1066.7	1120	108.9	98.1	2537	3.2	3.0
520	1484.9	1011.5	1130	189.1	169.5	2941	4.4	4.0
530	1572.4	1084.9	1137	132.2	118.7	2973	7.6	7.0
540	1550.7	1082.4	1161	339.0	301.9	3005	6.5	6.0
550	1561.5	1102.2	1180	460.0	406.8	3056	3.2	3.0
570	1501.5	1087.4	1200	423.6	375.2	3132	5.4	5.0
590	1395.5	1024.3	1235	480.5	423.6	3156	19.4	18.0
610	1485.3	1088.8	1290	413.1	365.7	3204	1.3	1.2
630	1434.1	1062.1	1320	250.2	223.4	3245	3.2	3.0
650	1419.9	1061.7	1350	32.5	30.1	3317	13.1	12.0
670	1392.3	1046.2	1395	1.6	1.4	3344	3.2	3.0
690	1130.0	859.2	1443	55.7	51.6	3450	13.3	12.2
710	1316.7	1002.4	1463	105.1	97.0	3573	11.9	11.0
718	1010.3	816.9	1477	105.5	97.3	3765	9.8	9.0
724	1043.2	842.8	1497	182.1	167.1	4045	7.5	6.9

Table 16.3 AM0 standard solar spectrum adapted with permission from the annual book of ASTM standards, Copyright ASTM [8]

λ [nm]	$E(\lambda)$ [Wm^{-2} μm^{-1}]	λ [nm]	$E(\lambda)$ [Wm^{-2} μm^{-1}]	λ [nm]	$E(\lambda)$ [Wm^{-2} μm^{-1}]	λ [nm]	$E(\lambda)$ [Wm^{-2} μm^{-1}]	λ [nm]	$E(\lambda)$ [Wm^{-2} μm^{-1}]	λ [nm]	$E(\lambda)$ [Wm^{-2} μm^{-1}]	λ [nm]	$E(\lambda)$ [Wm^{-2} μm^{-1}]	λ [nm]	$E(\lambda)$ [Wm^{-2} μm^{-1}]	λ [nm]	$E(\lambda)$ [Wm^{-2} μm^{-1}]
–	–	–	–	–	–	–	–	–	–	–	–	–	–	–	–	–	–
119.5	6.30E − 2	320.5	820.6	521.5	1939	719.8	1388.0	1088	577.8	1490	296.2	1892	137.0	2294	67.99	4460	5.799
120.5	5.72E − 1	321.5	713	522.5	1855	720.7	1385.0	1090	599.3	1492	294.1	1894	135.3	2296	68.52	4480	5.694
121.5	5.00E + 0	322.5	701.8	523.5	1927	721.7	1386.0	1092	592.8	1494	296.2	1896	132.5	2298	68.39	4500	5.591
122.5	1.21E + 0	323.5	674	524.5	1992	722.7	1383.0	1094	555.9	1496	287.2	1898	137.1	2300	68.75	4520	5.491
123.5	4.86E − 2	324.5	775.4	525.5	1963	723.6	1389.0	1096	570.7	1498	291.2	1900	136.0	2302	68.89	4540	5.392
124.5	3.50E − 2	325.5	892.6	526.5	1702	724.6	1384.0	1098	569.5	1500	290.7	1902	138.9	2304	68.78	4560	5.296
125.5	2.94E − 2	326.5	998.3	527.5	1860	725.5	1372.0	1100	583.2	1502	278.9	1904	135.9	2306	68.64	4580	5.202
126.5	3.59E − 2	327.5	971	528.5	1930	726.5	1375.0	1102	570.4	1504	274.6	1906	136.5	2308	68.48	4600	5.110
127.5	2.17E − 2	328.5	935.2	529.5	1951	727.4	1374.0	1104	576.9	1506	271.9	1908	135.3	2310	68.08	4620	5.020
128.5	1.76E − 2	329.5	1081	530.5	1986	728.4	1347.0	1106	576.0	1508	281.1	1910	136.2	2312	68.00	4640	4.932
129.5	4.07E − 2	330.5	1036	531.5	1997	729.3	1332.0	1108	573.2	1510	288.8	1912	133.0	2314	67.98	4660	4.846
130.5	1.23E − 1	331.5	984.2	532.5	1801	730.3	1364.0	1110	573.0	1512	283.3	1914	135.5	2316	67.05	4680	4.762
131.5	4.06E − 2	332.5	973.2	533.5	1956	731.2	1358.0	1112	564.6	1514	281.1	1916	134.2	2318	66.42	4700	4.680
132.5	4.21E − 2	333.5	939.3	534.5	1890	732.2	1360.0	1114	565.3	1516	282.5	1918	133.5	2320	67.15	4720	4.599
133.5	1.71E − 1	334.5	977.3	535.5	2024	733.1	1351.0	1116	565.9	1518	283.3	1920	131.1	2322	65.70	4740	4.520
134.5	4.66E − 2	335.5	961.4	536.5	1903	734.0	1364.0	1118	563.6	1520	282.2	1922	133.5	2324	64.33	4760	4.443
135.5	3.88E − 2	336.5	825	537.5	1914	735.0	1348.0	1120	552.0	1522	274.6	1924	131.4	2326	64.30	4780	4.367
136.5	3.15E − 2	337.5	858	538.5	1937	735.9	1335.0	1122	561.0	1524	276.6	1926	132.3	2328	65.51	4800	4.293
137.5	2.98E − 2	338.5	939.2	539.5	1864	736.9	1337.0	1124	557.6	1526	280.5	1928	128.8	2330	65.65	4820	4.221
138.5	4.04E − 2	339.5	976.5	540.5	1800	737.8	1333.0	1126	543.3	1528	281.0	1930	128.5	2332	64.89	4840	4.150
139.5	7.71E − 2	340.5	1026	541.5	1913	738.8	1292.0	1128	550.8	1530	269.3	1932	126.8	2334	65.23	4860	4.080
140.5	6.19E − 2	341.5	941.5	542.5	1857	739.7	1309.0	1130	542.6	1532	278.0	1934	128.8	2336	64.33	4880	4.012
141.5	4.29E − 2	342.5	1012	543.5	1911	740.7	1295.0	1132	545.9	1534	272.8	1936	128.5	2338	64.06	4900	3.946
142.5	4.77E − 2	343.5	968.8	544.5	1911	741.6	1286.0	1134	542.1	1536	276.5	1938	128.9	2340	64.87	4920	3.881
143.5	5.21E − 2	344.5	810.9	545.5	1934	742.6	1307.0	1136	546.0	1538	273.3	1940	124.5	2342	64.77	4940	3.817

(*continued overleaf*)

Table 16.3 (*continued*)

λ [nm]	$E(\lambda)$ [Wm^{-2} μm^{-1}]	λ [nm]	$E(\lambda)$ [Wm^{-2} μm^{-1}]	λ [nm]	$E(\lambda)$ [Wm^{-2} μm^{-1}]	λ [nm]	$E(\lambda)$ [Wm^{-2} μm^{-1}]	λ [nm]	$E(\lambda)$ [Wm^{-2} μm^{-1}]	λ [nm]	$E(\lambda)$ [Wm^{-2} μm^{-1}]	λ [nm]	$E(\lambda)$ [Wm^{-2} μm^{-1}]	λ [nm]	$E(\lambda)$ [Wm^{-2} μm^{-1}]	λ [nm]	$E(\lambda)$ [Wm^{-2} μm^{-1}]
144.5	5.19E − 2	345.5	957.2	546.5	1911	743.5	1324.0	1138	534.1	1540	267.8	1942	126.0	2344	64.61	4960	3.754
145.5	5.64E − 2	346.5	944.1	547.5	1865	744.4	1309.0	1140	529.4	1542	270.3	1944	115.2	2346	64.23	4980	3.693
146.5	7.22E − 2	347.5	919	548.5	1895	745.4	1324.0	1142	531.8	1544	274.2	1946	113.6	2348	64.24	5000	3.633
147.5	8.65E − 2	348.5	914.4	549.5	1928	746.3	1316.0	1144	531.1	1546	273.6	1948	123.7	2350	64.13	5050	3.519
148.5	8.36E − 2	349.5	906.9	550.5	1894	747.3	1322.0	1146	538.2	1548	266.0	1950	123.5	2352	61.50	5100	3.387
149.5	8.11E − 2	350.5	1070	551.5	1903	748.2	1320.0	1148	533.9	1550	265.4	1952	119.8	2354	61.29	5150	3.261
150.5	8.86E − 2	351.5	998.3	552.5	1878	749.2	1297.0	1150	532.2	1552	268.9	1954	125.8	2356	62.34	5200	3.142
151.5	9.44E − 2	352.5	925.3	553.5	1914	750.1	1299.0	1152	529.2	1554	260.5	1956	125.0	2358	61.44	5250	3.028
152.5	1.19E − 1	353.5	1052	554.5	1931	752.0	1285.0	1154	531.3	1556	262.7	1958	124.7	2360	62.23	5300	2.919
153.5	1.32E − 1	354.5	1132	555.5	1930	754.0	1285.0	1156	526.4	1558	263.7	1960	123.7	2362	62.47	5350	2.814
154.5	2.10E − 1	355.5	1065	556.5	1853	756.0	1280.0	1158	525.4	1560	262.8	1962	122.6	2364	62.16	5400	2.715
155.5	2.19E − 1	356.5	929.8	557.5	1878	758.0	1271.0	1160	513.6	1562	264.5	1964	118.8	2366	62.07	5450	2.620
156.5	1.88E − 1	357.5	811.3	558.5	1818	760.0	1257.0	1162	506.8	1564	261.4	1966	120.7	2368	61.96	5500	2.529
157.5	1.75E − 1	358.5	706.9	559.5	1839	762.0	1260.0	1164	512.0	1566	257.5	1968	122.9	2370	61.18	5550	2.442
158.5	1.71E − 1	359.5	1010	560.5	1875	764.0	1243.0	1166	511.9	1568	256.2	1970	121.7	2372	61.47	5600	2.358
159.5	1.79E − 1	360.5	989.4	561.5	1856	766.0	1239.0	1168	513.9	1570	257.5	1972	117.9	2374	59.19	5650	2.279
160.5	1.97E − 1	361.5	895	562.5	1882	768.0	1224.0	1170	505.4	1572	258.9	1974	119.8	2376	61.03	5700	2.202
161.5	2.27E − 1	362.5	1017	563.5	1893	770.0	1215.0	1172	512.5	1574	253.4	1976	120.6	2378	61.37	5750	2.129
162.5	2.57E − 1	363.5	1016	564.5	1886	772.0	1206.0	1174	511.8	1576	244.7	1978	116.9	2380	61.05	5800	2.059
163.5	2.90E − 1	364.5	1033	565.5	1829	774.0	1205.0	1176	497.6	1578	241.6	1980	117.9	2382	60.29	5850	1.992
164.5	3.03E − 1	365.5	1174	566.5	1861	776.0	1186.0	1178	494.6	1580	256.2	1982	118.0	2384	57.17	5900	1.927
165.5	4.39E − 1	366.5	1256	567.5	1920	778.0	1207.0	1180	506.7	1582	246.8	1984	117.9	2386	57.25	5950	1.865
166.5	4.07E − 1	367.5	1203	568.5	1841	780.0	1212.0	1182	499.5	1584	250.2	1986	114.4	2388	59.29	6000	1.806
167.5	3.95E − 1	368.5	1122	569.5	1892	782.0	1206.0	1184	482.7	1586	251.0	1988	118.6	2390	59.41	6050	1.749
168.5	4.64E − 1	369.5	1249	570.5	1800	784.0	1207.0	1186	497.8	1588	240.0	1990	118.2	2392	59.09	6100	1.694
169.5	5.99E − 1	370.5	1161	571.5	1855	786.0	1202.0	1188	481.0	1590	228.5	1992	116.4	2394	59.10	6150	1.641
170.5	6.74E − 1	371.5	1197	572.5	1925	788.0	1191.0	1190	490.3	1592	243.6	1994	114.1	2396	58.90	6200	1.591

171.5	7.01E − 1	372.5	1074	573.5	1908	790.0	1174.0	1192	494.5	1594	251.3	1996	115.7	2398	59.22	6250	1.542
172.5	7.39E − 1	373.5	937.8	574.5	1899	792.0	1149.0	1194	493.7	1596	241.0	1998	114.5	2400	58.33	6300	1.495
173.5	7.79E − 1	374.5	917.6	575.5	1862	794.0	1166.0	1196	486.2	1598	250.9	2000	115.9	2402	58.82	6350	1.450
174.5	9.24E − 1	375.5	1082	576.5	1878	796.0	1161.0	1198	464.1	1600	243.5	2002	114.6	2404	58.60	6400	1.407
175.5	1.10E + 0	376.5	1106	577.5	1889	798.0	1152.0	1200	476.9	1602	243.9	2004	113.7	2406	58.32	6450	1.365
176.5	1.24E + 0	377.5	1306	578.5	1814	800.0	1143.0	1202	486.2	1604	243.5	2006	113.4	2408	58.21	6500	1.325
177.5	1.43E + 0	378.5	1353	579.5	1860	802.0	1139.0	1204	466.6	1606	242.1	2008	114.5	2410	58.13	6550	1.286
178.5	1.57E + 0	379.5	1087	580.5	1870	804.0	1137.0	1206	480.8	1608	244.3	2010	113.9	2412	58.09	6600	1.249
179.5	1.61E + 0	380.5	1225	581.5	1885	806.0	1130.0	1208	458.7	1610	232.5	2012	113.4	2414	55.61	6650	1.213
180.5	1.87E + 0	381.5	1103	582.5	1905	808.0	1110.0	1210	468.9	1612	237.9	2014	112.5	2416	54.02	6700	1.178
181.5	2.28E + 0	382.5	806.5	583.5	1889	810.0	1095.0	1212	474.0	1614	240.5	2016	112.7	2418	56.76	6750	1.145
182.5	2.29E + 0	383.5	697.2	584.5	1892	812.0	1091.0	1214	474.8	1616	228.9	2018	112.3	2420	56.40	6800	1.112
183.5	2.29E + 0	384.5	978.1	585.5	1814	814.0	1110.0	1216	474.7	1618	240.2	2020	110.7	2422	56.59	6850	1.081
184.5	2.11E + 0	385.5	1028	586.5	1862	816.0	1080.0	1218	471.7	1620	230.9	2022	108.6	2424	56.16	6900	1.051
185.5	2.36E + 0	386.5	1026	587.5	1880	818.0	1076.0	1220	469.4	1622	235.6	2024	110.3	2426	56.11	6950	1.022
186.5	2.75E + 0	387.5	1023	588.5	1780	820.0	1069.0	1222	468.0	1624	238.6	2026	110.3	2428	56.05	7000	0.994
187.5	3.07E + 0	388.5	1003	589.5	1640	822.0	1053.0	1224	465.6	1626	237.7	2028	109.4	2430	56.28	7050	0.967
188.5	3.35E + 0	389.5	1196	590.5	1844	824.0	1072.0	1226	464.8	1628	239.7	2030	106.8	2432	55.96	7100	0.941
189.5	3.64E + 0	390.5	1271	591.5	1818	826.0	1068.0	1228	457.4	1630	235.9	2032	109.4	2434	55.49	7150	0.916
190.5	3.84E + 0	391.5	1367	592.5	1839	828.0	1060.0	1230	461.5	1632	234.7	2034	107.7	2436	54.93	7200	0.892
191.5	4.25E + 0	392.5	1039	593.5	1827	830.0	1033.0	1232	457.9	1634	231.9	2036	107.6	2438	54.89	7250	0.868
192.5	4.19E + 0	393.5	593.4	594.5	1804	832.0	1047.0	1234	457.2	1636	229.0	2038	104.7	2440	55.47	7300	0.845
193.5	3.88E + 0	394.5	1046	595.5	1813	834.0	1028.0	1236	456.4	1638	222.4	2040	107.7	2442	55.25	7350	0.823
194.5	5.31E + 0	395.5	1339	596.5	1836	836.0	1019.0	1238	456.5	1640	221.6	2042	106.9	2444	55.10	7400	0.802
195.5	5.53E + 0	396.5	870.9	597.5	1811	838.0	1038.0	1240	449.7	1642	221.1	2044	107.2	2446	53.86	7450	0.781
196.5	6.12E + 0	397.5	946.6	598.5	1788	840.0	1017.0	1242	448.5	1644	220.7	2046	106.9	2448	53.35	7500	0.761
197.5	6.31E + 0	398.5	1552	599.5	1805	842.0	1020.0	1244	446.4	1646	226.6	2048	105.9	2450	53.20	7550	0.742
198.5	6.31E + 0	399.5	1695	600.1	1786	844.0	990.7	1246	447.5	1648	226.9	2050	105.8	2452	53.13	7600	0.723
199.5	6.79E + 0	400.5	1714	601.1	1762	846.0	1001.0	1248	446.6	1650	222.3	2052	104.3	2454	53.73	7650	0.705

(*continued overleaf*)

Table 16.3 (*continued*)

λ [nm]	$E(\lambda)$ [Wm^{-2} μm^{-1}]	λ [nm]	$E(\lambda)$ [Wm^{-2} μm^{-1}]	λ [nm]	$E(\lambda)$ [Wm^{-2} μm^{-1}]	λ [nm]	$E(\lambda)$ [Wm^{-2} μm^{-1}]	λ [nm]	$E(\lambda)$ [Wm^{-2} μm^{-1}]	λ [nm]	$E(\lambda)$ [Wm^{-2} μm^{-1}]	λ [nm]	$E(\lambda)$ [Wm^{-2} μm^{-1}]	λ [nm]	$E(\lambda)$ [Wm^{-2} μm^{-1}]	λ [nm]	$E(\lambda)$ [Wm^{-2} μm^{-1}]
200.5	7.47E + 0	401.5	1780	602.1	1740	848.0	1003.0	1250	446.5	1652	222.8	2054	104.7	2456	52.76	7700	0.688
201.5	8.18E + 0	402.5	1793	603.1	1784	850.0	967.0	1252	439.6	1654	224.8	2056	104.7	2458	52.11	7750	0.671
202.5	8.42E + 0	403.5	1716	604.1	1797	852.0	957.1	1254	441.3	1656	224.5	2058	104.0	2460	53.62	7800	0.654
203.5	9.39E + 0	404.5	1706	605.1	1791	854.0	867.9	1256	438.4	1658	224.3	2060	102.0	2462	53.43	7850	0.638
204.5	10.450	405.5	1699	606.1	1772	856.0	939.2	1258	436.8	1660	221.9	2062	103.9	2464	53.40	7900	0.623
205.5	10.740	406.5	1619	607.1	1776	858.0	984.8	1260	436.9	1662	222.6	2064	99.7	2466	53.12	7950	0.608
206.5	11.290	407.5	1659	608.0	1751	860.0	959.0	1262	433.6	1664	221.1	2066	103.1	2468	53.06	8000	0.593
207.5	12.900	408.5	1768	609.0	1740	862.0	975.9	1264	432.2	1666	217.7	2068	102.3	2470	51.39	8050	0.579
208.5	15.340	409.5	1747	610.0	1728	864.0	912.5	1266	430.7	1668	214.5	2070	100.3	2472	52.84	8100	0.565
209.5	21.790	410.5	1561	611.0	1740	866.0	878.8	1268	424.0	1670	219.8	2072	101.2	2474	51.77	8150	0.552
210.5	28.450	411.5	1849	612.0	1730	868.0	953.1	1270	430.4	1672	210.8	2074	101.7	2476	52.51	8200	0.539
211.5	34.180	412.5	1820	613.0	1720	870.0	951.1	1272	428.7	1674	215.6	2076	101.3	2478	52.12	8250	0.527
212.5	31.900	413.5	1786	614.0	1685	872.0	944.2	1274	424.5	1676	208.5	2078	101.0	2480	49.95	8300	0.514
213.5	33.790	414.5	1766	615.0	1712	874.0	947.1	1276	426.0	1678	211.7	2080	98.7	2482	49.96	8350	0.503
214.5	40.800	415.5	1763	616.0	1661	876.0	949.1	1278	423.6	1680	202.0	2082	99.9	2484	51.60	8400	0.491
215.5	36.840	416.5	1874	616.9	1644	878.0	925.3	1280	416.7	1682	198.6	2084	98.0	2486	49.72	8450	0.480
216.5	32.890	417.5	1693	617.9	1700	880.0	926.3	1282	373.2	1684	207.8	2086	99.5	2488	51.24	8500	0.469
217.5	35.960	418.5	1713	618.9	1699	882.0	914.5	1284	408.6	1686	208.6	2088	99.1	2490	51.23	8550	0.459
218.5	45.220	419.5	1730	619.9	1715	884.0	928.3	1286	413.1	1688	208.3	2090	98.9	2492	51.06	8600	0.448
219.5	47.820	420.5	1788	620.9	1727	886.0	913.5	1288	413.7	1690	206.4	2092	95.6	2494	50.48	8650	0.438
220.5	48.240	421.5	1828	621.9	1698	888.0	915.4	1290	409.5	1692	209.8	2094	96.5	2496	50.64	8700	0.429
221.5	40.330	422.5	1609	622.9	1697	890.0	911.5	1292	412.3	1694	208.4	2096	96.1	2498	50.45	8750	0.419
222.5	50.600	423.5	1740	624.8	1664	892.0	902.6	1294	409.3	1696	207.7	2098	96.8	2500	50.61	8800	0.410
223.5	64.220	424.5	1798	625.8	1662	894.0	905.5	1296	411.4	1698	206.8	2100	96.7	2520	49.22	8850	0.401
224.5	60.100	425.5	1724	626.8	1709	896.0	910.5	1298	406.5	1700	203.4	2102	96.3	2540	47.82	8900	0.393
225.5	53.290	426.5	1727	627.8	1715	898.0	885.7	1300	408.3	1702	201.8	2104	96.4	2560	46.46	8950	0.384
226.5	40.160	427.5	1596	628.8	1712	900.0	880.8	1302	403.2	1704	202.1	2106	96.4	2580	45.15	9000	0.376
227.5	40.690	428.5	1614	629.8	1685	902.0	882.7	1304	400.4	1706	202.4	2108	95.9	2600	43.89	9050	0.368

228.5	52.940	429.5	1501	630.7	1682	904.0	872.8	1306	403.4	1708	199.0	2110	94.0	2620	42.68	9100	0.360
229.5	48.620	430.5	1155	631.7	1649	906.0	872.8	1308	401.6	1710	200.3	2112	95.1	2640	41.50	9150	0.353
230.5	53.120	431.5	1715	632.7	1684	908.0	846.1	1310	399.9	1712	192.3	2114	94.7	2660	40.37	9200	0.345
231.5	51.950	432.5	1674	633.7	1662	910.0	857.0	1312	390.1	1714	201.0	2116	92.9	2680	39.28	9250	0.338
232.5	54.280	433.5	1760	634.7	1673	912.0	864.9	1314	397.3	1716	198.7	2118	93.9	2700	38.22	9300	0.331
233.5	45.600	434.5	1698	635.7	1668	914.0	857.0	1316	384.9	1718	198.0	2120	92.8	2720	37.20	9350	0.324
234.5	39.710	435.5	1752	636.6	1663	916.0	852.0	1318	393.1	1720	195.0	2122	93.0	2740	36.21	9400	0.318
235.5	52.400	436.5	1962	637.6	1688	918.0	853.0	1320	394.2	1722	194.8	2124	91.5	2760	35.26	9450	0.311
236.5	49.520	437.5	1837	638.6	1682	920.0	827.3	1322	391.2	1724	188.4	2126	92.0	2780	34.34	9500	0.305
237.5	49.370	438.5	1594	639.6	1645	922.0	820.3	1324	391.6	1726	192.4	2128	92.6	2800	33.45	9550	0.299
238.5	42.770	439.5	1857	640.6	1633	924.0	826.3	1326	388.0	1728	191.5	2130	92.0	2820	32.59	9600	0.293
239.5	44.970	440.5	1742	641.5	1626	926.0	831.2	1328	386.8	1730	192.5	2132	92.1	2840	31.75	9650	0.287
240.5	40.310	441.5	1964	642.5	1642	928.0	837.2	1330	379.1	1732	188.7	2134	91.7	2860	30.95	9700	0.281
241.5	52.460	442.5	2014	643.5	1635	930.0	832.2	1332	379.5	1734	179.2	2136	89.6	2880	30.17	9750	0.276
242.5	71.960	443.5	1942	644.5	1637	932.0	840.1	1334	385.9	1736	174.6	2138	91.2	2900	29.41	9800	0.270
243.5	67.810	444.5	2007	645.5	1621	934.0	827.3	1336	382.9	1738	180.7	2140	90.6	2920	28.68	9850	0.265
244.5	62.140	445.5	1853	646.4	1622	936.0	812.4	1338	380.5	1740	185.6	2142	90.5	2940	27.97	9900	0.260
245.5	50.340	446.5	1924	647.4	1633	938.0	820.3	1340	375.4	1742	183.9	2144	89.8	2960	27.28	9950	0.255
246.5	51.370	447.5	2112	648.4	1634	940.0	813.4	1342	378.5	1744	186.9	2146	89.0	2980	26.62	10 000	0.250
247.5	56.570	448.5	2007	649.4	1570	942.0	798.5	1344	378.5	1746	183.0	2148	89.6	3000	25.97	11 000	0.170
248.5	46.530	449.5	2062	650.3	1630	944.0	814.4	1346	375.7	1748	182.2	2150	89.2	3020	25.35	12 000	0.119
249.5	57.460	450.5	2180	651.3	1645	946.0	809.4	1348	376.4	1750	182.7	2152	88.5	3040	24.74	13 000	8.65E − 2
250.5	61.250	451.5	2145	652.3	1618	948.0	793.6	1350	370.2	1752	181.7	2154	88.3	3060	24.15	14 000	6.42E − 2
251.5	46.890	452.5	1974	653.3	1605	950.0	795.6	1352	373.4	1754	183.7	2156	88.1	3080	23.58	15 000	4.86E − 2
252.5	42.340	453.5	2004	654.3	1589	952.0	788.6	1354	371.8	1756	182.8	2158	87.8	3100	23.03	16 000	3.75E − 2
253.5	52.540	454.5	2013	655.2	1537	954.0	777.7	1356	361.6	1758	182.4	2160	87.0	3120	22.49	17 000	2.93E − 2
254.5	60.710	455.5	2069	656.2	1303	956.0	791.6	1358	368.6	1760	181.8	2162	86.0	3140	21.97	18 000	2.33E − 2
255.5	80.820	456.5	2112	657.2	1456	958.0	788.6	1360	363.4	1762	176.6	2164	84.2	3160	21.47	19 000	1.87E − 2
256.5	103.800	457.5	2136	658.2	1567	960.0	784.7	1362	365.9	1764	179.4	2166	75.6	3180	20.98	20 000	1.52E − 2
257.5	127.800	458.5	2005	659.1	1563	962.0	779.3	1364	361.3	1766	180.5	2168	82.6	3200	20.50	25 000	6.28E − 3
258.5	127.500	459.5	2043	660.1	1580	964.0	777.2	1366	364.0	1768	178.5	2170	84.7	3220	20.04	30 000	3.04E − 3

(*continued overleaf*)

Table 16.3 (*continued*)

λ [nm]	$E(\lambda)$ [$\mathrm{Wm^{-2}\,\mu m^{-1}}$]	λ [nm]	$E(\lambda)$ [$\mathrm{Wm^{-2}\,\mu m^{-1}}$]	λ [nm]	$E(\lambda)$ [$\mathrm{Wm^{-2}\,\mu m^{-1}}$]	λ [nm]	$E(\lambda)$ [$\mathrm{Wm^{-2}\,\mu m^{-1}}$]	λ [nm]	$E(\lambda)$ [$\mathrm{Wm^{-2}\,\mu m^{-1}}$]	λ [nm]	$E(\lambda)$ [$\mathrm{Wm^{-2}\,\mu m^{-1}}$]	λ [nm]	$E(\lambda)$ [$\mathrm{Wm^{-2}\,\mu m^{-1}}$]	λ [nm]	$E(\lambda)$ [$\mathrm{Wm^{-2}\,\mu m^{-1}}$]	λ [nm]	$E(\lambda)$ [$\mathrm{Wm^{-2}\,\mu m^{-1}}$]
259.5	106.000	460.5	2075	661.1	1585	966.0	767.2	1368	358.4	1770	177.1	2172	85.0	3240	19.59	35 000	1.64E – 3
260.5	87.150	461.5	2090	662.0	1597	968.0	771.7	1370	356.4	1772	177.8	2174	85.1	3260	19.15	40 000	9.65E – 4
261.5	91.520	462.5	2140	663.0	1569	970.0	767.5	1372	359.3	1774	177.7	2176	84.1	3280	18.72	50 000	3.97E – 4
262.5	105.600	463.5	2075	664.0	1558	972.0	771.9	1374	357.4	1776	174.3	2178	82.7	3300	18.31	60 000	1.92E – 4
263.5	168.900	464.5	2010	665.0	1575	974.0	754.1	1376	352.6	1778	173.0	2180	84.8	3320	17.91	80 000	6.10E – 5
264.5	254.500	465.5	2077	665.9	1567	976.0	760.4	1378	356.3	1780	173.3	2182	82.9	3340	17.52	1 00 000	2.51E – 5
265.5	257.500	466.5	1954	666.9	1555	978.0	756.1	1380	355.6	1782	172.7	2184	84.1	3360	17.14	1 20 000	1.21E – 5
266.5	254.200	467.5	2049	667.9	1554	980.0	752.4	1382	351.4	1784	172.5	2186	84.0	3380	16.77	1 50 000	4.98E – 6
267.5	255.600	468.5	2028	668.8	1569	982.0	755.1	1384	353.8	1786	171.5	2188	81.2	3400	16.41	2 00 000	1.58E – 6
268.5	248.500	469.5	2024	669.8	1554	984.0	749.2	1386	349.4	1788	173.4	2190	82.7	3420	16.06	2 50 000	6.51E – 7
269.5	243.500	470.5	1909	670.8	1551	986.0	745.6	1388	351.5	1790	171.7	2192	83.2	3440	15.72	3 00 000	3.06E – 7
270.5	272.400	471.5	2052	671.8	1541	988.0	742.9	1390	348.1	1792	170.4	2194	82.8	3460	15.39	4 00 000	1.05E – 7
271.5	228.700	472.5	2076	672.7	1537	990.0	732.0	1392	349.3	1794	168.9	2196	82.5	3480	15.07	10 00 000	3.51E – 9
272.5	201.200	473.5	2025	673.7	1533	992.0	738.7	1394	347.0	1796	168.8	2198	82.5	3500	14.76	10 00 000	3.51E – 9
273.5	200.200	474.5	2086	674.7	1530	994.0	737.6	1396	345.3	1798	168.5	2200	82.1	3520	14.45	–	–
274.5	135.200	475.5	2050	675.6	1527	996.0	733.6	1398	346.8	1800	167.6	2202	81.6	3540	14.16	–	–
275.5	178.500	476.5	1990	676.6	1523	998.0	731.4	1400	339.2	1802	164.5	2204	81.7	3560	13.87	–	–
276.5	247.500	477.5	2110	677.6	1520	1000.0	728.0	1402	340.3	1804	166.6	2206	77.4	3580	13.58	–	–
277.5	238.200	478.5	2043	678.5	1518	1002.0	725.8	1404	338.1	1806	165.5	2208	79.3	3600	13.31	–	–
278.5	162.300	479.5	2111	679.5	1515	1004.0	709.7	1406	337.9	1808	165.3	2210	80.6	3620	13.04	–	–
279.5	87.190	480.5	2070	680.5	1513	1006.0	685.9	1408	338.5	1810	164.9	2212	80.5	3640	12.78	–	–
280.5	96.450	481.5	2126	681.4	1510	1008.0	714.5	1410	338.2	1812	163.1	2214	80.2	3660	12.53	–	–
281.5	212.300	482.5	2058	682.4	1508	1010.0	713.4	1412	329.6	1814	161.3	2216	79.2	3680	12.28	–	–
282.5	299.800	483.5	2053	683.4	1506	1012.0	709.5	1414	330.7	1816	156.9	2218	79.2	3700	12.04	–	–
283.5	319.500	484.5	2003	684.3	1504	1014.0	702.9	1416	333.3	1818	145.6	2220	79.5	3720	11.80	–	–
284.5	239.800	485.5	1862	685.3	1503	1016.0	697.1	1418	332.9	1820	155.8	2222	79.1	3740	11.57	–	–
285.5	166.300	486.5	1653	686.3	1501	1018.0	694.6	1420	329.7	1822	154.6	2224	78.8	3760	11.35	–	–
286.5	328.900	487.5	1862	687.2	1500	1020.0	691.0	1422	321.9	1824	159.4	2226	77.1	3780	11.13	–	–
287.5	342.800	488.5	1947	688.2	1499	1022.0	687.5	1424	325.9	1826	159.3	2228	78.0	3800	10.92	–	–

288.5	328.400	489.5	1994	689.1	1506	1024.0	694.0	1426	320.2	1828	157.1	2230	77.9	3820	10.71	–	–
289.5	481.800	490.5	2041	690.1	1512	1026.0	691.4	1428	319.5	1830	158.5	2232	77.9	3840	10.50	–	–
290.5	612.800	491.5	1929	691.1	1506	1028.0	690.5	1430	321.0	1832	157.0	2234	77.8	3860	10.31	–	–
291.5	592.000	492.5	1929	692.0	1495	1030.0	680.2	1432	322.4	1834	156.1	2236	77.3	3880	10.11	–	–
292.5	531.900	493.5	1921	693.0	1495	1032.0	682.3	1434	321.5	1836	156.1	2238	75.7	3900	9.92	–	–
293.5	545.800	494.5	2093	694.0	1498	1034.0	664.4	1436	322.5	1838	154.0	2240	76.2	3920	9.74	–	–
294.5	518.500	495.5	1959	694.9	1480	1036.0	675.4	1438	323.1	1840	154.3	2242	76.1	3940	9.56	–	–
295.5	563.800	496.5	2051	695.9	1489	1038.0	665.5	1440	308.8	1842	151.3	2244	76.2	3960	9.38	–	–
296.5	519.400	497.5	2052	696.8	1489	1040.0	664.4	1442	314.5	1844	152.5	2246	76.1	3980	9.21	–	–
297.5	517.000	498.5	1898	697.8	1457	1042.0	664.3	1444	311.6	1846	153.5	2248	74.7	4000	9.04	–	–
298.5	474.400	499.5	2004	698.8	1494	1044.0	666.3	1446	317.4	1848	147.2	2250	75.5	4020	8.87	–	–
299.5	493.300	500.5	1889	699.7	1486	1046.0	651.0	1448	314.7	1850	153.0	2252	75.0	4040	8.69	–	–
300.5	428.000	501.5	1843	700.7	1462	1048.0	655.3	1450	312.2	1852	151.8	2254	73.7	4060	8.52	–	–
301.5	464.300	502.5	1927	701.6	1455	1050.0	656.5	1452	308.0	1854	150.5	2256	74.2	4080	8.35	–	–
302.5	498.300	503.5	1967	702.6	1462	1052.0	653.4	1454	307.9	1856	148.0	2258	74.5	4100	8.18	–	–
303.5	632.500	504.5	1901	703.6	1468	1054.0	647.3	1456	306.6	1858	149.8	2260	74.3	4120	8.02	–	–
304.5	614.000	505.5	2027	704.5	1482	1056.0	650.1	1458	311.8	1860	147.2	2262	72.6	4140	7.87	–	–
305.5	606.200	506.5	1995	705.5	1472	1058.0	633.3	1460	309.6	1862	146.0	2264	73.5	4160	7.71	–	–
306.5	566.400	507.5	1939	706.4	1452	1060.0	634.8	1462	306.0	1864	146.6	2266	72.9	4180	7.56	–	–
307.5	626.800	508.5	1952	707.4	1455	1062.0	640.7	1464	305.5	1866	144.1	2268	73.2	4200	7.42	–	–
308.5	623.200	509.5	1949	708.3	1442	1064.0	633.8	1466	303.7	1868	144.1	2270	73.1	4220	7.27	–	–
309.5	506.000	510.5	1980	709.3	1426	1066.0	627.2	1468	304.5	1870	145.4	2272	72.6	4240	7.13	–	–
310.5	634.300	511.5	2031	710.3	1440	1068.0	621.4	1470	302.3	1872	140.7	2274	72.1	4260	7.00	–	–
311.5	743.200	512.5	1899	711.2	1416	1070.0	611.3	1472	300.6	1874	136.6	2276	72.5	4280	6.86	–	–
312.5	668.500	513.5	1893	712.2	1408	1072.0	620.4	1474	295.8	1876	119.0	2278	72.3	4300	6.74	–	–
313.5	713.300	514.5	1906	713.1	1408	1074.0	611.3	1476	296.4	1878	139.0	2280	71.9	4320	6.61	–	–
314.5	675.600	515.5	1933	714.1	1413	1076.0	610.6	1478	294.1	1880	140.3	2282	68.8	4340	6.48	–	–
315.5	645.100	516.5	1697	715.0	1398	1078.0	606.6	1480	300.0	1882	142.1	2284	71.1	4360	6.36	–	–
316.5	645.300	517.5	1755	716.0	1403	1080.0	616.9	1482	297.5	1884	141.3	2286	70.8	4380	6.25	–	–
317.5	788.800	518.5	1682	716.9	1407	1082.0	588.3	1484	293.2	1886	138.5	2288	71.0	4400	6.13	–	–
318.5	677.600	519.5	1860	717.9	1400	1084.0	596.4	1486	296.0	1888	141.4	2290	70.8	4420	6.02	–	–
319.5	724.100	520.5	1863	718.8	1376	1086.0	607.3	1488	273.1	1890	137.6	2292	70.5	4440	5.91	–	–

technologies and as long as methods for the correlation between results using the reference spectrum and results from "real world" spectra is established. The technical basis for the direct spectra has recently been reexamined and found to have a diffuse component that is substantially greater than that concentrators would normally encounter [19, 20]. On examination of the US solar radiation database, it was found that when the global-normal irradiance is near 1000 Wm^{-2}, the direct-normal component is near 850 Wm^{-2} and not the 767 Wm^{-2} that the direct standard spectrum integrates into [20]. This difference has been attributed to an aerosol optical depth at 500 nm of 0.27 in the terrestrial reference spectra [20]. This has not been a problem for single junction PV concentrators in the past because of their relative insensitivity to the specific direct spectra [21]. Recent high-efficiency structures such as the GaInP/GaAs/Ge triple-junction solar cell exhibit a significant difference in the efficiency between the global and direct reference spectrum (>10% relative) [22, 23] as shown in Figure 16.2. It has been proposed that the direct reference spectrum be modified to have a lower aerosol optical depth of 0.066 broadband or 0.085 at 500 nm to better represent the spectral irradiance in sunny regions (average daily direct-beam energy greater than 6 $kWh/m^2/day$) where concentrators might be deployed [22]. This low aerosol optical depth direct beam reference spectrum was generated using the same atmospheric conditions as the current terrestrial reference spectrum [10, 12, 13, 18] and has been adopted at NREL for evaluating concentrators as of January 2003. Tabular values of this direct beam spectrum can be found at the following web sites: *http://www.nrel.gov/highperformancepv/* or *http://rredc.nrel.gov/solar/standards/am1.5/*.

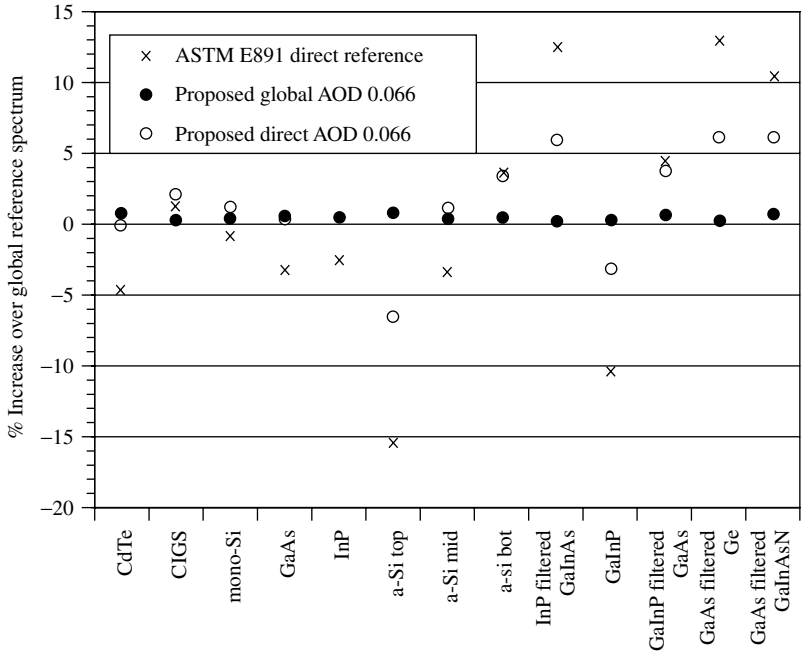

Figure 16.2 Percentage change in the normalized short-circuit current from the normalized global reference spectrum for various state-of-the-art PV technologies compared with the proposed direct reference spectra

The extraterrestrial spectral irradiance distribution at one astronomical unit distance from the sun is commonly referred to as the AM0 spectrum. At present, international consensus standards do not exist for AM0 measurements. Each country's space agency has adopted its own internal procedures. However, an international standard is in the draft stage [15]. Measurements of the total AM0 irradiance used by the aerospace community have varied from 1353 Wm^{-2} to 1372 Wm^{-2} [8, 14, 16, 24, 25]. Many groups still rely on the less accurate value of 1353 Wm^{-2} total AM0 irradiance [16, 24]. Recently, a new ASTM AM0 standard has been adopted that uses more accurate spectral irradiance measurements that are given in Table 16.3 and Figure 16.1 [8]. The best estimate for the solar "constant" is 1367 Wm^{-2} recommended by the World Radiation Center [14] or 1366.1 recommended by ASTM [8]. Both of these values were obtained from long-term monitoring of the solar irradiance with an active-cavity radiometer on the Solar Max and Nimbus 7 and other satellites [26]. Fortunately, the 1353 Wm^{-2} total AM0 irradiance, used by many groups for efficiency measurements and reporting purposes does not enter into the spacecraft PV power measurements. This is because primary balloon or space-based AM0 reference cells are calibrated at whatever irradiance that exists at the time of calibration, corrected to one astronomical unit distance from the sun. This means that numerical values of the AM0 total irradiance and spectral irradiance are not used in calibrating primary AM0 reference cells as discussed in Section 16.3.3.

A variety of definitions for cells and modules have been proposed [1, 5, 27, 28]. A module consists of several encapsulated, environmentally protected, and electrically interconnected cells. The area of a cell is taken to be the total area of the space charge region which includes grids and contacts. The standard cell area definitions replace the term *space charge region* with frontal area, but this term does not adequately account for devices with multiple cells on a single substrate or superstrate. The area of a concentrator cell is based upon the cell area that is designed to be illuminated [5]. This area is taken to be the area of the space charge region minus the area of any peripheral bus bars or contacts. A submodule or minimodule is an unencapsulated module.

The PV efficiency (η) is inversely proportional to the area definition used (equation 16.1). In fact, differences in the area definition often account for the greatest differences in η between various groups and values published in the literature [28, 29]. The largest differences occur when the so-called active area (total device area minus all area that is shaded or not active) is used. The use of an active area in the efficiency neglects the trade-off between lower resistance losses and increased shading. Several thin-film PV device structures do not have any shading losses, so the active and total area is the same. To prevent an artificial increase in the efficiency, care must be taken to ensure that light outside the defined area cannot be collected by multiple internal reflections or that carriers generated outside the defined area are collected due to incomplete electrical isolation. The smaller the cell area, the larger this possible effect. The larger the perimeter-to-area ratio, the greater the effect of the current being collected outside the defined area. This phenomenon is the reason a 1-cm^2 minimum area is required for inclusion in the *Progress in Photovoltaics* efficiency tables [30]. To be sure that the region enclosed by the total area is the only active region, an aperture should be used [30]. At the module level, the total area including the frame is used. For prototype modules, where the frame design is less important than the encapsulation and cell interconnections, an aperture-area definition is often used. The aperture-area definition is the total area minus the frame area.

This aperture area may be defined by opaque tape if there is no frame to eliminate the possibility of the module collecting current outside the defined aperture area by multiple internal reflections or light piping.

The most common performance rating method for modules is the PV power conversion efficiency under SRC (Table 16.1). The power or peak watt rating on the module's nameplate is usually given with respect to SRC, as shown in Table 16.1 using a 25°C module temperature. Unfortunately, prevailing conditions under natural sunlight do not commonly match nameplate conditions. The nameplate rating that the manufacturer assigns to a given module model number is often higher than the measured power output in the field [31–33]. If the nameplate rating is determined at 25°C, then the actual power produced is often less than this because the module will typically run at 40° to 60°C. The temperature coefficient for the peak power is usually negative. The nameplate rating also does not include long-term degradation or system losses. System losses include the power-conditioning unit's efficiency, ability of the power conditioner to operate at the maximum PV power point, orientation, shading, resistance losses in the wiring, and mismatch in the power of different modules.

The nominal operating cell temperature (NOCT) is a rating designed to give information about the thermal qualities of a module and a more realistic estimate of the power in the field on a sunny day at solar noon. The NOCT of a module is a fixed temperature that the module would operate at if it is exposed to the nominal thermal environment (20°C air temperature, 800 Wm^{-2} total irradiance, and a wind speed of 1 ms^{-1}) [7, 34]. The term "standard operating conditions" or SOC is sometimes used for flat-plate or concentrator-terrestrial modules operating at NOCT. The actual determination of the NOCT of a module with an uncertainty of less than ±2°C has proved difficult because of difficulties in measuring the temperature of cells in an encapsulated module, uncertainties in the total irradiance, and secondary environmental effects such as wind direction, ground reflections, mounting, and electrical loading [34, 35]. The installed NOCT is up to 15°C warmer for roof-mounted applications than a free-standing module depending on the stand off distance between the module and the roof [34, 35]. The module temperature can be calculated from the NOCT or installed NOCT and air temperature using

$$T = T_{\text{air}} + (\text{NOCT} - 20^{\circ}\text{C})E_{\text{tot}}/800\ \text{Wm}^{-2}. \tag{16.2}$$

A wind speed correction can also be applied to equation (16.2) [7, 34].

For a fair and meaningful comparison of efficiencies between technologies, the measurements should be performed after any initial degradation. Commercial silicon modules have shown small changes in performance after the first few hours of operation [36, 37]. At the present time, all amorphous silicon PV technologies degrade when exposed to sunlight. Fortunately, this degradation stabilizes at a level of 80% to 90% of the initial value (see Chapter 12). Partial recovery occurs in the field during the summer when the higher module temperature leads to partial annealing or when amorphous silicon modules are annealed in the laboratory at 60° to 70°C [38, 39]. The efficiency continues to decrease after 500 h of light exposure at lower temperatures even if the light level is reduced [38–40]. For a fair and meaningful comparison of improvements in amorphous silicon module development, the performance at SRC is now reported after illumination

of about 1000 Wm^{-2}, at a module back-surface temperature of nominally 50°C, for at least 1000 h, with a resistive load near P_{max}, and low humidity [28, 39]. These conditions were chosen to approximate one year of outdoor exposure without the humidity or temperature cycling. Other thin-film module technologies may undergo reversible and irreversible changes during the first few hours of light exposure [29, 41, 42].

16.2.2 Alternative Peak Power Ratings

A variety of groups have suggested and adopted alternative rating schemes to compare module and system performance between the various PV technologies. These schemes are based on measurements of a module's performance in the field and on performing a regression analysis on the data. The site-specific power production is more relevant for bulk power generation than the power with respect to a particular theoretical reference spectrum and module operating temperature.

One popular method was adopted by Pacific Gas and Electric Company and the Photovoltaics for Utility-Scale Applications (PVUSA) project in California, USA, to rate and purchase PV systems. They perform a linear regression analysis on the actual measured system or module power produced (P), air temperature (T_a), wind speed (S), and total plane-of-array irradiance (E_{tot}) as measured with a pyranometer or radiometer:

$$P = P_{max}(E_{tot}, T_a, S) = E_{tot}(C_1 + C_2 E_{tot} + C_3 T_a + C_4 S), \tag{16.3}$$

where C_1, C_2, C_3, and C_4 are the regression coefficients [32, 43]. The goal of performing a multiple regression analysis on the measured power to a fixed set of environmental conditions is to accurately represent the average power output under clear-sky conditions near midday at a given site. The power can be measured at the maximum direct-current (DC) power point, or on the DC side of the inverter, or at the alternating-current (AC) power out of the inverter. The last two power measurement locations will include some system losses. This site-specific rating scheme takes into account the different thermal characteristics of modules and spectral sensitivities since it is not referenced to a standard spectrum or module temperature. The power rating is evaluated using equation (16.3) at $T_a = 20°C$, $S = 1\ ms^{-1}$, and $E_{tot} = 1000\ Wm^{-2}$ for flat-plate collectors. For concentrators, the direct-normal incidence sunlight within a 5° or 5.7° field of view of 850 Wm^{-2} is used for E_{tot}. The difference between the fields of view is because an absolute-cavity radiometer has a 5° field of view and some less accurate but less expensive normal incidence pyrheliometers have a 5.7° field of view.

The primary advantage of basing the reference temperature on the air temperature is that the different thermal characteristics of the module, array, and system are included in the rating, and the power rating is closer to what is actually observed. The different spectral conditions at the different sites are also accounted for by not referencing the performance to a fixed spectrum, but rather, referencing the power to the actual spectrum that was incident on the module. If a PV reference cell is used to measure E_{tot}, then the power would be with respect to a reference spectrum at all light levels. Spectral mismatch issues associated with E_{tot}, measured with a thermal- or spectrally matched detector are discussed further in Section 16.3.1.

16.2.3 Energy-based Performance Rating Methods

Despite its widespread acceptance, the peak power rating (i.e. maximum instantaneous watts) does not capture the differences among the plethora of flat-plate and concentrator-module designs with different total irradiance, diffuse irradiance, spectral irradiance, and temperature sensitivities. Energy-based ratings (i.e. integrated power over time in kWh) capture the module performance in the "real" world. It is easy to integrate the measured PV power produced over a time interval to obtain the total energy produced compared with the incident energy. A variety of rating criteria besides the standard reference conditions listed in Table 16.1 exist, depending on the application in Table 16.4.

The AM/PM method, proposed by ARCO/Siemens Solar Industries, attempts to rate a module in terms of the PV energy produced during a standard solar day with a given reference temperature and total irradiance distribution [44]. The AM/PM method is appealing because it is an energy-rating method that is not site-specific. A variation on the AM/PM energy-rating method was developed in which a regression analysis of the measured power and irradiance data to a nonlinear response function was summed over a standard day defined by a fourth-order polynomial [45].

A rating scheme based on the PV energy delivered over a standard day has been proposed for a small set of standard days [46–49]. These five days were obtained from the typical meteorological year database (*http://rredc.nrel.gov/solar/old_data/*) corresponding to a hot-sunny, cold-sunny, hot-cloudy, cold-cloudy, and a nice day [49, 50]. The meteorological data for the standard days include latitude, longitude, date, air temperature, wind speed, relative humidity, and direct, diffuse-horizontal, and global-normal irradiances. The direct-beam and plane-of-array spectral irradiances were then computed for hourly intervals throughout the day using a spectral model [51]. The model developed by Nann requires only the meteorological parameters listed in the standard days. Figure 16.3 shows the meteorological characteristics of the hot-sunny standard day [46–49]. The hot-sunny day was taken from the meteorological data for Phoenix Arizona, US, on June 24, 1976 [49, 50].

Other schemes for energy rating based on site-specific conditions instead of standard days have also been developed. In 1990, a rating based on realistic reporting conditions (RRC) was proposed. This method measured the performance of PV modules under different irradiances and temperatures and predicted the module's output under

Table 16.4 Photovoltaic rating criterion for PV applications

Application	Relevant PV parameter
Grid-connected, hydrogen production	Annual energy delivered
Power for peak utility demand	Power near solar noon
Remote system for cooling	Temperature coefficient and NOCT
Remote system with storage	Energy during cloudy day
Pump system for agriculture	Energy during growing season
Small power consumer products	Efficiency at very low irradiance
High value (Space)	High efficiency, radiation, and thermal stability

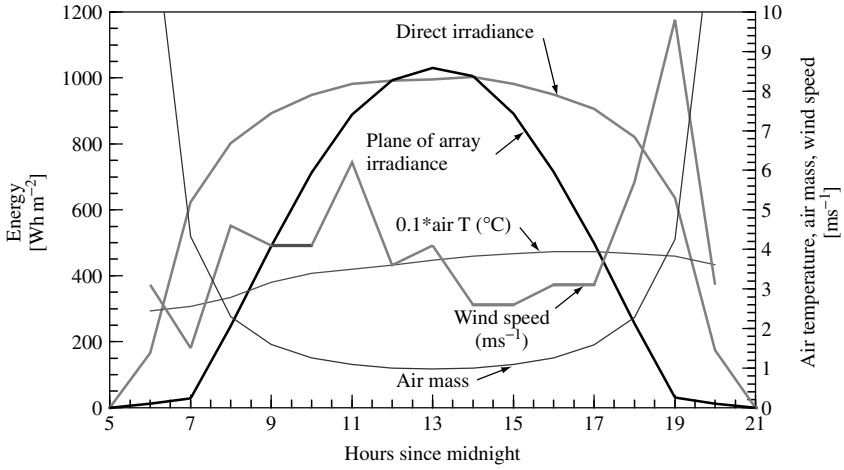

Figure 16.3 Meteorological conditions for the hot-sunny reference day [46–49]

various operating conditions [3, 4, 52–54]. This method has been used to compare commercial modules, highlighting the different dependencies on light level and temperature. Figure 16.4 illustrates the comparative ratings of selected modules for various locations in the United States [52] and Europe [53]. The results in Figure 16.4 indicate that the annual PV efficiency is 2 to 20% less than the efficiency under SRC (25°C, 1000 Wm^{-2}, and the global reference spectrum). The annual PV efficiency is total PV energy divided by the total energy deposited on a south-facing surface tilted to the latitude of the site. Spectral effects were ignored in Figure 16.4 with the global reference spectrum in Table 16.2 used for all calculations, so only temperature and total irradiance effects are included. The solar cell was modeled as described in Chapter 3 with a double exponential with series resistance and shunt resistance to model the performance as a function of total irradiance and temperature. Current state-of-the-art modules may be less sensitive to temperature and irradiance variations because of smaller temperature coefficients, series resistance, dark current, and a larger shunt resistance. The deviation of the annual efficiency from the efficiency under SRC would have been less if two-axis tracking were assumed. However, most flat-plate systems do not employ two-axis tracking. The spectral model developed by Nann was coupled with a PV model to compare the performance of a variety of PV technologies [4]. The PV model used a double exponential with series and shunt resistances to fit to the highest-efficiency cells made at the time of each technology. The environmental conditions include time, date, global-horizontal irradiance, direct-normal irradiance, diffuse irradiance, plane-of-array irradiance, ambient temperature, wind speed, and relative humidity. The results of the study were similar to those summarized in Figure 16.4 and References [52, 53]. The spectral model confirmed that the spectral sensitivity of Si, CdTe, $CuInSe_2$, and GaAs technologies on the annual energy production is $+1\%$ to -3%. The results also show that the efficiency of single- and multijunction amorphous silicon is $\sim$10% less in winter months solely from spectral effects [4].

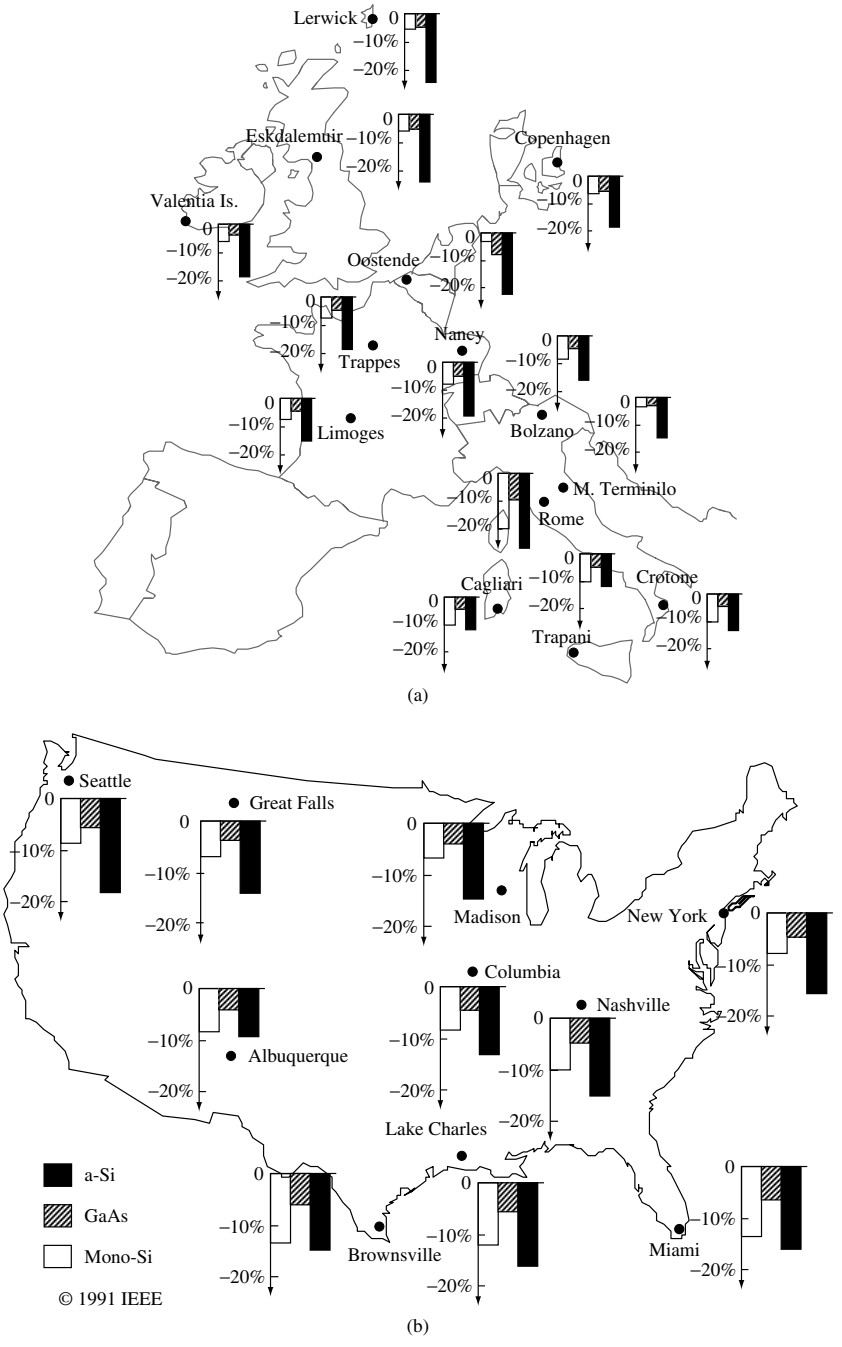

Figure 16.4 Example of PV performance on a yearly basis normalized to standard reference conditions for three different solar cell technologies (a-Si, GaAs, and c-Si) showing the percentage of deviation from standard conditions for a variety of locations in (a) Europe [52] and (b) the United States [53]

16.2.4 Translation Equations to Reference Conditions

The most basic translation equations for a solar cell are based on the diode model with series and shunt resistances discussed in Chapters 3 and 7. This model has been extended to modules by combining them in series and parallel combinations [55].

To a first order, short-circuit current (I_{SC}), open-circuit voltage (V_{OC}), P_{max}, and fill factor (FF) are linear with temperature, whereas the current is linear with E_{tot} [49, 56–60]. These linear translation equations allow the performance under standard reference conditions to be translated to other conditions for energy-based rating methods. Typical temperature coefficients for various PV technologies are summarized in Table 16.5 and Figure 16.5.

A set of translation equations for current and voltage based on the work of Sandstrom has been implemented in consensus standards [61, 62]. These equations translate the entire current versus voltage ($I-V$) curve for temperature and irradiance. Following the notation of the international standard in Reference [62], the following equations allow one to translate the current I_1 and voltage V_1 measured from temperature T_1 to T_2 and irradiance E_1 to E_2:

$$I_2 = I_1 + I_{SC1}\left(\frac{E_2}{E_1} - 1\right) + \alpha(T_2 - T_1) \tag{16.4}$$

$$V_2 = V_1 - R_s(I_2 - I_1) - I_2K(T_2 - T_1) + \beta(T_2 - T_1), \tag{16.5}$$

where α and β are the temperature coefficients, R_s is the series resistance, and K is a curve-shape correction factor. Applying equations (16.4) and (16.5) at a fixed irradiance

Table 16.5 Typical Si solar cell temperature coefficients [57]

Type	$-V_{OC}$ [ppm/°C]	I_{SC} [ppm/°C]	$-FF$ [ppm/°C]	$-P_{max}$ [ppm/°C]
Si cells & modules	2400–4500	400–980	940–1700	2600–5500

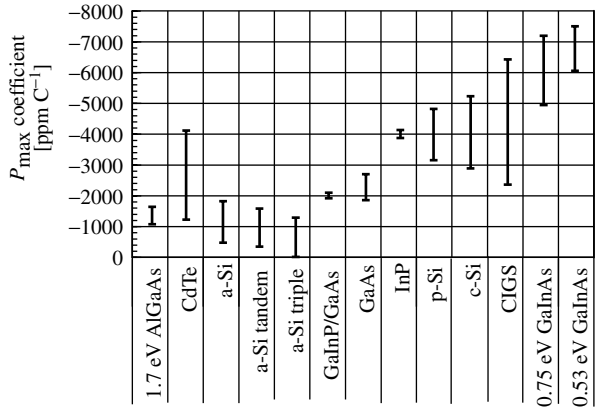

Figure 16.5 Typical P_{max} temperature coefficients of various PV technologies [57]

($E_2 = E_1$) and assuming no series resistance ($R_s = 0$), the value of K that best translates the $I-V$ characteristics for temperature is determined.

Translation equations for I_{SC}, V_{OC}, V_{max}, and I_{max} as a function of E_{tot}, T_c, absolute air mass (AM_a), and angle of incidence (AOI) based on multiple regression analysis of field data have been proposed by King [63]:

$$I_{SC}(E, T_c, AM_a, AOI) = (E/E_0) f_1(AM_a) f_2(AOI)[I_{SC0} + \alpha_{I_{SC}}(T_c - T_o)] \tag{16.6}$$

$$E_e = I_{SC}(E, T_c = T_0, AM_a, AOI)/I_{SC0} \tag{16.7}$$

$$I_{mp}(E_e, T_c) = C_0 + E_{ec}[C_1 + \alpha_{I_{mp}}(T_c - T_0)] \tag{16.8}$$

$$V_{OC}(E_e, \mathrm{i}) = V_{OC0} + C_2 \ln(E_e) + \beta_{V_{OC}}(T_c - T_0) \tag{16.9}$$

$$V_{mp}(E_e, T_c) = V_{mp0} + C_3 \ln(E_e) + C_4[\ln(E_e)]^2 + \beta_{V_{mp}}(T_c - T_0) \tag{16.10}$$

$$I_{SC0} = I_{SC}(E = E_0, T_c = T_0, AM_a = 1.5, AOI = 0^\circ) \tag{16.11}$$

$$V_{OC0} = V_{OC}(E_e = 1, T_c = T_0) \tag{16.12}$$

$$V_{mp0} = V_{mp}(E_e = 1, T_c = T_0) \tag{16.13}$$

$$f_2 = \frac{\dfrac{E_0}{I_{SC0}} I_{SC}(AM_a = 1.5, T_c = T_0) - E_{diff}}{E_{dir}\cos(\theta)}, \tag{16.14}$$

where E is the plane-of-array solar irradiance, E_e is the effective irradiance in units of suns, E_0 is the one-sun irradiance of 1000 Wm^{-2}, E_{diff} is the diffuse irradiance in the plane of the module, E_{dir} is the direct-normal irradiance, and AOI is the solar angle of incidence on the module; T_c is the temperature of the cells inside the module, T_0 is the module reference temperature, and $\alpha_{I_{SC}}$, α_{Imp}, $\beta_{V_{OC}}$, and $\beta_{V_{mp}}$ are the temperature coefficients of I_{SC}, I_{mp}, V_{OC}, and V_{mp}, respectively. These temperature coefficients are in absolute units so they will vary with the size of the PV device, the number of devices in series, or the number of devices in parallel. The pressure-corrected relative optical air mass AM_a can be written as [64]

$$AM_a = \frac{P}{P_0}[\cos(\theta) + 0.50572(96.07995^\circ - \theta)^{-1.6364}]^{-1}, \tag{16.15}$$

where P is the barometric pressure, P_0 is the pressure at sea level, and θ is the angle between the sun and zenith in degrees. The function $f_1(AM_a)$ is empirically obtained from the temperature- and irradiance-corrected I_{SC} versus air mass and assumes that the only spectral dependence is the zenith angle. Data are collected over a range of irradiances, incident angles, air masses, and temperatures and a multiple regression analysis is applied. These translation equations have been compared with simple linear translation equations derived from simulator-based measurements for several modules using outdoor data [49]. These translation equations give similar results to equation (16.3) when temperature, maximum-power tracking, and spectral issues are considered [48]. Other translation equations for current and voltage are possible [16, 65].

16.3 CURRENT VERSUS VOLTAGE MEASUREMENTS

A solar cell can be modeled as a diode in parallel with a current generator, whereas a module is a series-parallel network of solar cells, as discussed in Chapter 7. Measurements of cell or module $I-V$ behavior allow the diode characteristics to be determined, along with other important parameters including the maximum-power point, $P_{\max}$. A typical $I-V$ measurement system is composed of a simulated or natural light source, test bed to mount the device under test, temperature control and sensors, and a data acquisition system to measure the current and voltage as the voltage across the device or current through the device is varied with an external load or power supply.

16.3.1 Measurement of Irradiance

Irradiance measurements are made with respect to a reference spectral irradiance or the prevailing solar spectral irradiance. The measurement of the irradiance, E_{tot}, incident on the PV device in equation (16.1) is typically performed with a thermal detector (pyranometer, cavity radiometer) for outdoor measurements and reference cells for simulator-based measurements. If the goal is to determine the PV efficiency or power with respect to standardized or different reference conditions, then a spectral error will exist. Outdoor measurements of PV systems or modules are often made with respect to the prevailing or total irradiance incident on the module. If a broadband thermal detector with a constant spectral responsivity is used, then the spectral error is zero. If a silicon-based pyranometer is used to measure the performance based on the total irradiance, then there will be a spectral error because Si does not respond over the entire spectrum. For PV measurements with respect to a reference spectrum, the spectral error in the measured short-circuit current I_{SC} of a PV device can be written in general as [2]:

$$I'_{\text{SC}} = \frac{I_{\text{SC}}}{M} = I_{\text{SC}} \frac{\int_{\lambda_1}^{\lambda_2}\int_{\theta_1}^{\theta_2}\int_{\phi_1}^{\phi_2} E_{\text{Ref}}(\lambda,\theta,\phi) S_{\text{T}}(\lambda,\theta,\phi)\,\mathrm{d}\lambda\mathrm{d}\theta\mathrm{d}\phi}{\int_{\lambda_1}^{\lambda_2}\int_{\theta_1}^{\theta_2}\int_{\phi_1}^{\phi_2} E_{\text{Ref}}(\lambda,\theta,\phi) S_{\text{R}}(\lambda,\theta,\phi)\,\mathrm{d}\lambda\mathrm{d}\theta\mathrm{d}\phi} \times \frac{\int_{\lambda_1}^{\lambda_2}\int_{\theta_1}^{\theta_2}\int_{\phi_1}^{\phi_2} E_{\text{S}}(\lambda,\theta,\phi) S_{\text{R}}(\lambda,\theta,\phi)\,\mathrm{d}\lambda\mathrm{d}\theta\mathrm{d}\phi}{\int_{\lambda_1}^{\lambda_2}\int_{\theta_1}^{\theta_2}\int_{\phi_1}^{\phi_2} E_{\text{S}}(\lambda,\theta,\phi) S_{\text{T}}(\lambda,\theta,\phi)\,\mathrm{d}\lambda\mathrm{d}\theta\mathrm{d}\phi}, \tag{16.16}$$

where the spectral responsivity of the device under test (S_{T}), spectral responsivity of the reference detector (S_{R}), reference spectral irradiance (E_{Ref}), and source spectral irradiance (E_{S}) are a function of wavelength (λ) and incident azimuth (ϕ) and zenith (θ) angles. This general form allows the reference detector to be noncoplanar with the device under test and the source angular distribution of the source spectrum to be nearly arbitrary. In practice, the test device and reference detector used to measure the total irradiance are usually coplanar to minimize errors associated with measuring the orientation. The

direct and AM0 reference spectra have no angular dependence, and measurements are normally performed at normal incidence, so the angular dependence in equation (16.16) drops out. If the angular dependence of the reference detector used to measure E_{tot} and the global reference spectra follow an ideal cosine response, then equation (16.16) simplifies to [66, 67]:

$$M = \frac{\int_{\lambda_1}^{\lambda_2} E_{\text{Ref}}(\lambda) S_{\text{R}}(\lambda)\, \text{d}\lambda}{\int_{\lambda_1}^{\lambda_2} E_{\text{Ref}}(\lambda) S_{\text{T}}(\lambda)\, \text{d}\lambda} \frac{\int_{\lambda_1}^{\lambda_2} E_{\text{S}}(\lambda) S_{\text{T}}(\lambda)\, \text{d}\lambda}{\int_{\lambda_1}^{\lambda_2} E_{\text{S}}(\lambda) S_{\text{R}}(\lambda)\, \text{d}\lambda}. \tag{16.17}$$

If the reference detector is a thermal detector, S_{R} is independent of the wavelength and drops out. The source spectral irradiance (E_{S}) and spectral responsivity of S_{R} and S_{T} need only be relative in equation (16.17), since any multiplicative error sources will drop out. Ideally, the limits of integration λ_1 and λ_2 in equation (16.17) should encompass the range of the reference detector and reference spectrum, or else an error can arise [68]. If the spectral irradiance of the light source is the same as the reference spectrum or if the relative spectral responsivity of the reference detector matches the relative spectral responsivity of the test device, then M is unity. Manufacturers of PV cells and modules for multimillion dollar satellites require the lowest possible measurement uncertainty; so they require primary balloon or space-calibrated reference cells of the same manufacturing lot, and purchase solar simulators with the closest spectral match to AM0 that is technically possible so that they can assume that M is unity.

The short-circuit current of the reference cell under the source spectrum ($I^{\text{R,S}}$) is used to determine the effective irradiance using the following equation:

$$E_{\text{tot}} = \frac{I^{\text{R,S}} M}{CV} \tag{16.18}$$

where CV is the calibration value of the instrument used to measure the incident irradiance in units of AW^{-1}m^2. If a thermal detector is used, then CV has the units of VW^{-1}m^2 and $S_{\text{R}}(\lambda)$ is constant.

16.3.2 Simulator-based $I-V$ Measurements: Theory

The short circuit current of a test device ($I^{\text{T,R}}$) at the reference total irradiance (E_{Ref}) can be written as [2, 4, 67]:

$$I^{\text{T,R}} = \frac{I^{\text{T,S}} E_{\text{Ref}} CV}{I^{\text{R,S}} M} \tag{16.19}$$

where $I^{\text{T,S}}$ is the short-circuit current of the test device measured under the source spectrum, M is from equation (16.17), and $I^{\text{R,S}}$ is the measured short-circuit current of the reference cell under the source spectrum. This is the standard simulator-based calibration procedure. Many groups assume M is unity because of the difficulty of obtaining a spectral irradiance of the source spectrum and knowledge of the spectral responsivities of the

test and reference device. Typically, the simulator is adjusted so that E_{tot} is equal to E_{Ref} from equation (16.18) or

$$I = \frac{E_{Ref} CV}{I^{R,S} M} = \frac{I^{R,R}}{I^{R,S} M} \tag{16.20}$$

where $I^{R,R}$ is the calibrated short-circuit current of the reference cell under the reference spectral and total irradiance. Typically, a reference cell is made of the same material and technology as the devices that it will be used to test, causing M to be closer to unity since $S_R \approx S_T$. Ideally, the angular response of the reference package should be similar to the device under test. This is essential for outdoor measurements [2, 69–71]. Consensus standards have been developed, giving guidance for reference cells [72–75]. If the detector package has a window and an air gap between the window and cell, then the package should be completely illuminated and used only with simulators to prevent reflection-related artifacts [29, 76]. Recently, the terrestrial community has proposed a standard package design for the World Photovoltaic Scale [74, 75]. This package was designed by international terrestrial PV calibration laboratories to accommodate their various PV calibration equipment, while having standardized connectors to facilitate international intercomparisons.

16.3.3 Primary Reference Cell Calibration Methods

Perhaps the most straightforward method of determining the short-circuit current with respect to a set of reference conditions is to measure the absolute external spectral responsivity of the test device at the reference temperature, $S_T(\lambda)$, and to integrate it with the reference spectrum, $E_{Ref}(\lambda)$, at the reference total irradiance, E_{tot}, using the following equation:

$$E_{tot} CV = I_{SC} = \frac{E_{tot} A \int_{\lambda_1}^{\lambda_2} E_{Ref}(\lambda) S_T(\lambda)\, d\lambda}{\int_{\lambda_1}^{\lambda_2} E_{Ref}(\lambda)\, d\lambda}. \tag{16.21}$$

For I_{SC} to be in units of A, wavelength (λ) must be in units of μm, PV area (A) in m^2, $E_{Ref}(\lambda)$ in $Wm^{-2}\mu m^{-1}$, E_{tot} in Wm^{-2}, and $S_T(\lambda)$ in AW^{-1}. The limits of integration should encompass the range of $E_{Ref}(\lambda)$. If $E_{Ref}(\lambda)$ is normalized to integrate to E_{tot}, then the limits of integration should encompass the response range of the device. The relationship between the spectral responsivity and the quantum yield is discussed in 16.4. Equation (16.21) assumes that $S_T(\lambda)$ is uniform over the PV device and that $S_T(\lambda)$ is independent of voltage bias, E_{tot}, and $E_{Ref}(\lambda)$. These assumptions can be relaxed for single-junction devices by applying an external bias light operating at E_{tot}. Several groups have gone to great lengths to minimize the various errors associated with equation (16.21) [77, 78]. Several intercomparisons show that differences of more than 10% in the absolute spectral response are possible from well-known PV calibration laboratories [74, 79–81]. Accurate spectral response measurements require measuring the

total power incident on a small area of the PV device (or the power density over the entire PV device) and the current produced at that wavelength. The major sources of uncertainty are the detector calibration used to measure the power (typically μW) and the errors in measuring a small AC current (typically μA or less) produced by the chopped monochromatic light, in the presence of a large DC offset (mA to A) from the broadband bias light. Because a reference cell calibrated using equation (16.21) will be fully illuminated when used to set a solar simulator or measure E_{tot} in natural sunlight, variations in the responsivity over the sample surface may result in an error in I_{SC}. Most groups use a high-current, low-noise operational amplifier with a gain of 10 to 10 000 as the current-to-voltage converter because commercial current amplifiers saturate around 10 mA. Some groups employ a laser to more accurately measure the absolute response of a reference cell at one wavelength because the light power is in the milliwatt range, instead of microwatt, associated with diffraction-grating or filter-based systems and because reference detectors used to measure the monochromatic light power can be more accurately calibrated for laser lines.

A primary reference cell can be calibrated under natural sunlight using equation (16.19) and a thermal detector [1, 2, 9, 66, 82, 83]:

$$CV = \frac{I^{\text{T,S}}}{E_{\text{tot}}} \frac{\int_{\lambda_1}^{\lambda_2} E_{\text{Ref}}(\lambda) S_{\text{T}}(\lambda)\, \text{d}\lambda}{\int_{\lambda_1}^{\lambda_2} E_{\text{Ref}}(\lambda)\, \text{d}\lambda} \frac{\int_{\lambda_1}^{\lambda_2} E_{\text{S}}(\lambda)\, \text{d}\lambda}{\int_{\lambda_1}^{\lambda_2} E_{\text{S}}(\lambda) S_{\text{T}}(\lambda)\, \text{d}\lambda} \tag{16.22}$$

where the cell short-circuit current ($I^{\text{T,S}}$) the solar spectra ($E_{\text{S}}(\lambda)$), and the total irradiance (E_{tot}) are measured at the same time. The spectral responsivity of the reference detector is constant, so $S_{\text{R}}(\lambda)$ is constant and drops out of equation (16.22). The incident irradiance E_{tot} is measured with a thermal detector that is traceable to the world radiometric reference scale, such as an absolute-cavity radiometer or pyranometer. The solar constant and solar power density in units of Wm^{-2} for solar applications are based on the world radiometric reference scale, which is derived from a family of primary absolute-cavity radiometers that are maintained at the World Radiation Research Center in Davos, Switzerland [84]. The field of view for the cell and spectroradiometer must be matched. Some investigators prefer to use a pyranometer mounted coplanar to the spectroradiometer and solar cell(s) on a horizontal surface [9, 85]. The investigators at the National Renewable Energy Laboratory (NREL) use an absolute-cavity radiometer because it is the primary instrument used to calibrate pyranometers and has a field of view of 5°, minimizing field-of-view-related error sources [1, 68, 82, 86]. A spectral model was developed to extend the measured direct-beam spectrum to encompass the limits of the reference spectra to minimize the errors in equation (16.21) [68, 83, 86]. The pyranometer-based calibration method requires the measurement of the spectral irradiance over a wavelength range of 300 to 2500 nm [9, 85]. Typically, CV is an average of many measurements taken over several days. This method only requires that the relative spectral response and spectral irradiance be known, thereby eliminating all error sources that are not wavelength-dependent.

If the absolute spectral irradiance $E_{\text{S}}(\lambda)$ of the light source in the test plane is known, as is the case for a standard lamp, black-body or absolute spectral irradiance

measurement, then equation (16.18) reduces to [66, 87–89]

$$CV = I^{\mathrm{T,S}} \frac{\displaystyle\int_{\lambda_1}^{\lambda_2} E_{\mathrm{Ref}}(\lambda) S_{\mathrm{T}}(\lambda)\, \mathrm{d}\lambda}{\displaystyle\int_{\lambda_1}^{\lambda_2} E_{\mathrm{Ref}}(\lambda)\, \mathrm{d}\lambda \int_{\lambda_1}^{\lambda_2} E_{\mathrm{S}}(\lambda) S_{\mathrm{T}}(\lambda)\, \mathrm{d}\lambda} \tag{16.23}$$

This method is appealing because the reference spectrum may correspond to the blackbody spectrum, and it can be readily performed in the laboratory. This method only requires the relative spectral responsivity measurements. If a standard lamp is used and the reference spectrum is the terrestrial reference spectra in Table 16.2, then the spectral correction factor in equation (16.23) is typically 12 [89]. Commercial standard lamps are typically 1000-W tungsten lamps supplied with an absolute spectral irradiance at a 50-cm distance and specific lamp current. This method is sensitive to errors in $S_{\mathrm{T}}(\lambda)$, $E_{\mathrm{S}}(\lambda)$, positioning, and stray light [68, 89]. The sensitivity to positioning is because the light source (i.e. standard lamp or black body) is not collimated and changes in the total irradiance of 1% per mm distance from the source are not uncommon [89]. If a solar simulator is used as the light source in equation (16.23), then the ratio of the integrals involving $S_{\mathrm{T}}(\lambda)$ approach unity minimizing the sensitivity to errors in $S_{\mathrm{T}}(\lambda)$, $E_{\mathrm{S}}(\lambda)$ and positioning errors are reduced to less than 0.1% per mm of distance from the source [87].

Once the short-circuit current is known under a given $E_{\mathrm{old}}(\lambda)$, it can be translated to any other $E_{\mathrm{new}}(\lambda)$ with the following equation:

$$I_{\mathrm{new}} = \frac{I_{\mathrm{old}} E_{\mathrm{tot}}^{\mathrm{new}}}{E_{\mathrm{tot}}^{\mathrm{old}}} \frac{\displaystyle\int_{\lambda_1}^{\lambda_2} E_{\mathrm{old}}(\lambda)\, \mathrm{d}\lambda}{\displaystyle\int_{\lambda_1}^{\lambda_2} E_{\mathrm{new}}(\lambda)\, \mathrm{d}\lambda} \frac{\displaystyle\int_{\lambda_1}^{\lambda_2} E_{\mathrm{new}}(\lambda) S_{\mathrm{T}}(\lambda)\, \mathrm{d}\lambda}{\displaystyle\int_{\lambda_1}^{\lambda_2} E_{\mathrm{old}}(\lambda) S_{\mathrm{T}}(\lambda)\, \mathrm{d}\lambda} \tag{16.24}$$

Equation (16.24) assumes that the current is linear with intensity. This method is especially useful for translating the calibration of primary AM0 reference cells to terrestrial reference spectra or vice versa.

The AM0 reference spectrum is by definition the extraterrestrial solar spectrum at one astronomical unit distance from the sun. This means that a small random error will exist because the solar spectrum varies slightly with solar activity. The AM0 community uses this fact to calibrate reference detectors by measuring their response in space or very high altitudes. By definition, there is no spectral error.

Extraterrestrial calibration procedures include using spacecraft, balloons, and high-altitude aircraft [15, 90–96]. There are no spectral corrections for balloon and spacecraft calibrations because the data are taken above the atmosphere. The high-altitude aircraft calibration procedure involves a Langley plot of the logarithm of I_{SC} versus absolute or pressure-corrected air mass over a typical range of 0.25 to 0.5 [92, 93, 95, 96]. The data are collected above the tropopause, thereby eliminating water vapor and most scattering, with the dominant spectral feature arising from ozone absorption [92, 96]. The Jet Propulsion Laboratory (JPL) balloon calibration program requires a custom package design for

standardized mounting, data acquisition system, and thermal considerations [90, 91]. See Chapter 10 for further discussion of calibration of reference cells for testing space cells.

16.3.4 Uncertainty Estimates in Reference Cell Calibration Procedures

All measurements have an uncertainty between the measured or derived value and the true value. In the case of terrestrial PV reference cell calibrations, the true value is the value under reference conditions given in Table 16.1. For extraterrestrial calibrations, the true value is determined by the actual solar spectrum, at the time of calibration and not the tabular reference spectrum, as in the case of terrestrial calibrations. Any variation in the primary AM0 calibration because of the varying solar constant is not considered an error. The spectral responsivity of PV cells change as a function of radiation damage. For an accurate assessment of the performance as a function of radiation damage using procedures that assume the spectral correction factor is unity, at least three matched reference cells are required (beginning of life, midlife, and end of life) to minimize the spectral errors.

The uncertainty that is expected to include 95% of results (U_{95}) in a calibration can be expressed in terms of the random error and systematic error component defined below, through the following equation [97]:

$$U_{95} \equiv \sqrt{B^2 + (t_{95}A)^2} \tag{16.25}$$

where A is the statistical component applied to a series of repeated determinations and is often expressed as a standard deviation. Type B error sources are associated with the instruments used in the measurement process and their associated calibration uncertainties. Student's t value for 95% coverage (t_{95}) is approximately 2.0 for an average of more than 20 measurements. The elemental error sources are composed of J random and systematic error components. The *systematic* error is

$$A \equiv \sqrt{\sum_{i=1}^{J} (\Theta_i A_i)^2} \tag{16.26}$$

The term *systematic error* is sometimes used synonymously with bias or nonrandom error. The sensitivity coefficient (Θ_i) is obtained by partial differentiation of the result with respect to one of the parameters in the result. If A_i is expressed in units of percent error, then Θ_i is unity. The *random* error is

$$B \equiv \sqrt{\sum_{i=1}^{J} (\Theta_i B_i)^2} \tag{16.27}$$

An example of an uncertainty analysis of equation (16.22) using the NREL direct-beam calibration method is given in Table 16.6 [98, 99]. Detailed uncertainty analysis using Monte Carlo methods indicates that the uncertainty in the spectral correction factor is 10%

Table 16.6 Uncertainty analysis of the tabular calibration method equation (16.22) [98]

Elemental error source	Systematic [±%]	Random [±%]	Total U_{95} [±%]
I_{SC} ($I^{T,S}$) measurement instrumentation	0.10	0.10	0.22
Absolute-cavity radiometer (E_{tot})	0.37	0.13	0.45
Spectral correction factor	0.20	0.20	0.45
Temperature correction & control @ ±1°C	0.15	0.05	0.18
$I^{T,S}$ linearity with varying E_{tot}	0.05	0.05	0.11
Thermal offset voltages	0.05	0.05	0.11
$I^{T,S}$ time constant different from radiometer	0.10	–	0.10
Total	0.47	0.27	0.72

to 20% of the magnitude of the spectral correction factor [68, 99]. A detailed uncertainty analysis of the error in determining the maximum power of a module measured outdoors using the ISO methodology was performed by Whitfield and Osterwald [100]. The ISO methodology has been adopted by all major calibration laboratories and replaces the previous ANSI methodology [101].

16.3.5 Intercomparison of Reference Cell Calibration Procedures

Typically, groups claiming to be able to calibrate primary reference cells with respect to reference conditions claim an uncertainty in the calibration value CV of ±1% [74, 80, 81, 94, 102]. Intercomparisons among the various calibration methods are the best way to determine if the uncertainty estimates are valid. Formal intercomparison of terrestrial calibration procedures sponsored by the Photovoltaic Energy Project (PEP) were conducted in 1985, 1987, and 1993 [74, 80, 81]. The PEP '85 intercomparison involved PV calibration laboratories from the Commission of European Communities, France, Germany, Italy, Japan, United Kingdom, and the United States. The differences in I_{SC} with respect to the global reference spectrum between the laboratories in the PEP '85 intercomparison were almost 8% for single-crystal and multicrystal silicon and 20% for amorphous silicon. However, in the PEP '85 intercomparison, six out of the eight agencies agreed within 3% for the crystalline cells and 6% for the amorphous cells [81]. In the PEP '87 and PEP '93 intercomparisons, the participants provided uncertainty estimates. The level of agreement between the laboratories for the PEP '87 intercomparison was 4% for single-crystal and multicrystal silicon cells and 14% for amorphous silicon [80]. This level of agreement was 2 to 10 times the labs' estimated uncertainties, which ranged from ±0.7% to ±5%, indicating that the uncertainty estimates for some of the participants were overly optimistic [80]. Several of the participants based their estimated uncertainties on the standard deviation of repeated calibrations thereby neglecting nonrandom error sources. The PEP '93 intercomparison also showed a rather large spread of 12% for the single-crystal and multicrystal silicon cells, even though the estimated U_{95} uncertainties ranged from ±1.0% to ±2.7%, again indicating that several laboratories underestimated their errors [74]. After excluding laboratories whose calibrations were based on reference cells and laboratories that had more than 50% of their calibrations exceed ±2% of the mean, the resultant average

deviation was 1.1% [74]. Because the terrestrial PV calibration laboratories around the world could not agree on a calibration procedure that had a proven U_{95} uncertainty of less than $\pm 2\%$, it was decided to establish a set of reference standards called the World Photovoltaic Scale (WPVS) [74, 75]. The four laboratories from the PEP '93 intercomparison that performed primary calibrations and were within $\pm 2\%$ of the mean were the NREL in the United States, Japan Quality Assurance Organization/Electrotechnical Laboratory in Japan, Tianjin Institute of Power Sources in the Peoples Republic of China, and Physikalisch-Technische Bundesanstalt (PTB) in Germany. A formal mechanism was established to include other laboratories in the future, provided their calibrations agreed with the four established WPVS calibration laboratories. The WPVS reference cells reside with the laboratory that provided them, providing each participating laboratory with reference cells traceable to the WPVS. A set of technical drawings was developed for future WPVS reference cells to prevent the problem with the existing set of 20 WPVS reference cells having incompatible cables, mounting holes, and temperature sensors [74, 75]. Sixteen of the 20 WPVS reference cells were recently recalibrated, along with six new candidate WPVS reference cells [102]. The new WPVS calibration values changed by 0.4% at most, with an average decrease of 0.2% [102]. The results of the PEP terrestrial intercomparisons were much closer than earlier intercomparisons, where deviations of $\pm 3\%$ were common and deviations of 5% from the mean were observed [103]. The year-to-year repeatability appeared to be no better than $\pm 3\%$ [103].

Surprisingly, the spread in I_{SC} temperature coefficients for the laboratories that performed them was greater than 50%, even though the temperature of the cells could be controlled and they had temperature sensors permanently attached to them [74]. This variation in temperature coefficient can be partly understood by noting that the temperature coefficient is a function of the light source that they are illuminated with [57]. For cells having a narrow response range, or for multijunction cells, the sign of the coefficient can even change depending on the light source [57, 104, 105].

The AM0 community has conducted intercomparisons between various groups over the years [90, 94, 106, 107]. In general, the agreement of primary AM0 calibrations on spacecraft, balloon, and high-altitude aircraft calibrations is better than $\pm 1\%$ over many years [90–92]. AM0 calibrations based on terrestrial measurements sometimes agree with primary high-altitude calibrations within 1% [91] and at other times the agreement is poor ($>10\%$) [106].

16.3.6 Multijunction Cell Measurement Procedures

Spectrum-splitting series-connected multijunction devices are critical to achieving high-efficiency III-V-based (Chapter 9) and a-Si-based (Chapter 12) solar cells. The procedures to measure the $I-V$ characteristics of a multijunction device with respect to reference conditions are the same as those for a single-junction device with the added constraint that the simulator should be set such that each junction operates at the proper photocurrent. This is accomplished by satisfying the following j equations for the j junctions in a multijunction PV device [108–111]:

$$I_j^{\mathrm{R,R}} = M_j I_j^{\mathrm{R,S}} \tag{16.28}$$

$$M_j = \frac{\int_{\lambda_1}^{\lambda_2} E_{\mathrm{Ref}}(\lambda) S_{\mathrm{R},j}(\lambda)\,\mathrm{d}\lambda \int_{\lambda_1}^{\lambda_2} E_{\mathrm{S}}(\lambda) S_{\mathrm{T},j}(\lambda)\,\mathrm{d}\lambda}{\int_{\lambda_1}^{\lambda_2} E_{\mathrm{Ref}}(\lambda) S_{\mathrm{T},j}(\lambda)\,\mathrm{d}\lambda \int_{\lambda_1}^{\lambda_2} E_{\mathrm{S}}(\lambda) S_{\mathrm{R},j}(\lambda)\,\mathrm{d}\lambda}. \tag{16.29}$$

This procedure involves adjusting the simulator in equation (16.28), measuring its spectrum, calculating M_j, and readjusting the simulator. If reference cells are used whose relative spectral responsivity efficiency matches each individual junction, then the spectral correction M_j is unity and only equation (16.27) needs to be satisfied. This is possible for the high-efficiency crystalline material systems in which the other junctions can be shorted out without significantly affecting the relative spectral responsivity [108]. The adjustment of the solar simulator to satisfy equation (16.28) can be problematic. Figure 16.6 illustrates the various approaches that researchers have taken in the past. The first approach illustrated in Figure 16.6(a) involves combining an ultraviolet (UV) light source L_1 and infrared (IR) light source L_2 with a dichroic filter assembly [108, 109, 112, 113]. This approach is particularly useful for two- and three-junction devices in which the top-cell energy gap is around 600 to 700 nm and the middle-cell energy gap is also around 600 to 700 nm. This is because of the relatively limited choices in the transition wavelength for standard dichroic filters. Figure 16.6(b) works for any material system because it uses

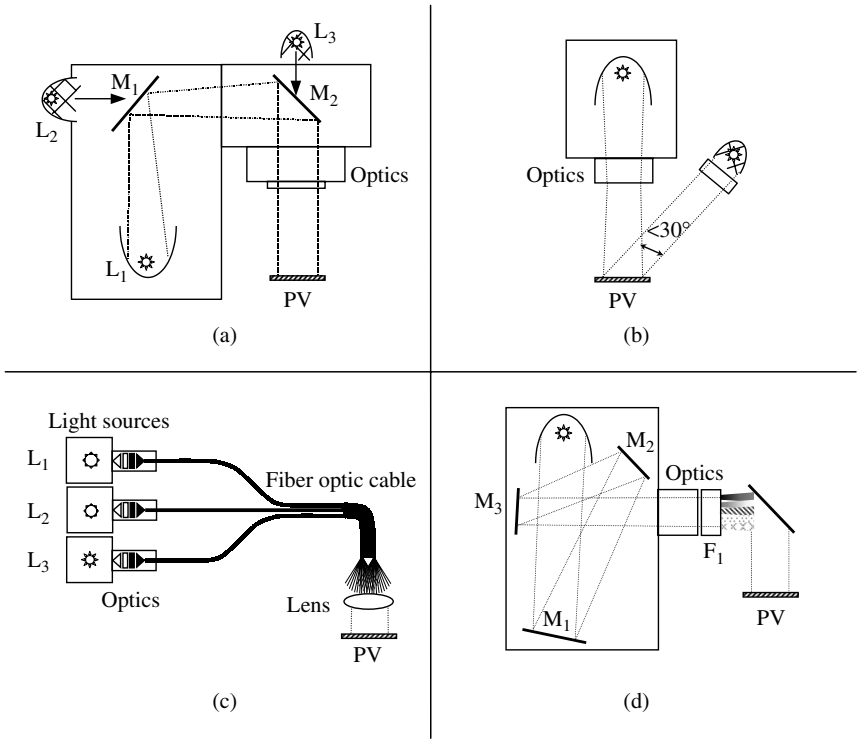

Figure 16.6 Methods of adjusting the spectral content of solar simulators. The light sources are L_1, L_2, and L_3 and the mirrors are M_1, M_2, and M_3

a simulator whose spectral match is close to the reference spectrum but brings in extra light that can be filtered at will for each junction [114]. The primary disadvantage of this approach is that the supplemental light sources are not collinear with the broadband light, giving the possibility of large variations in the spectral irradiance in the test plane. A fiber-optic solar simulator shown schematically in Figure 16.5(c) is useful because a wide variety of laser and incoherent light sources can be combined into one fiber bundle, which then illuminates the test plane [110, 115, 116]. This approach has the disadvantage of being restricted to small illumination areas, typically less than 2 cm in diameter at one sun. Another approach shown in Figure 16.6(d) is to place filters and apertures close to the integration optics of a large-area solar simulator [110, 114, 115]. This method is particularly useful for large-area (>100 cm^2) samples. Its primary drawback is that the light sources are not separately adjustable for each junction. This concept can also be applied to pulsed simulators, where the distance between the flash lamp(s) and the test plane is usually large and a wide range of intensities is possible. This method works for any multijunction technology because standard high-pass, low-pass, and band-pass filters are available to cover any combination of band gaps.

An entirely new procedure has recently been developed in which the light sources are set only once [111, 117, 118]. The approach is based on a simulator setup with multiple light sources arranged so that the intensity of each source may be adjusted without causing a change in the relative spectral irradiance. Each light source, $E_{S,i}(\lambda)$ for each junction, j can therefore be characterized by its relative irradiance. The adjustment of the intensity of the ith light source to an absolute level is mathematically described by the scaling factor C_i. Under these premises, the condition $I_j^{T,S} = I_j^{T,R}$ yields a system of j linear equations,

$$\sum_i C_i \int E_{S,i}(\lambda) S_{T,j}(\lambda)\, d\lambda = \int E_{ref}(\lambda) S_{T,j}(\lambda)\, d\lambda \tag{16.30}$$

which can easily be solved for the unknown scaling factors C_i. The intensity of the ith light source $E_{S,i}(\lambda)$ for the jth junction of the test device $S_{t,j}(\lambda)$ is adjusted until the measured short-circuit current of reference cell $I_j^{T,R}$ with an absolute spectral response $S_{R,j}(\lambda)$ is obtained using

$$I_j^{T,R} = C_i A \int E_{S,i}(\lambda) S_{R,j}(\lambda)\, d\lambda \tag{16.31}$$

The system of equations requires only relative spectral responses and relative irradiances and is therefore equivalent to the calculation of the mismatch factor in equation (16.29). The equations allow for the same reference cell to be used to set the simulator sources [111, 117, 118]. This procedure only requires one adjustment of each light source. This procedure also requires that the relative spectral irradiance be measured only once for each light source unlike the procedure described by equations (16.28) and (16.29), which requires a spectral irradiance measurement after each simulator adjustment. This allows the performance of a multijunction PV device under varying reference spectra or current-matching conditions to be rapidly determined.

16.3.7 Cell and Module $I-V$ Systems

A wide variety of $I-V$ measurement systems have been developed to measure the performance of PV devices, from 0.01-cm^2 area cells to multikilowatt arrays [2, 119]. A generic $I-V$ system is shown in Figure 16.7. The voltage across the PV device (from a cell to an array) is biased with a variable load, with the current being sensed by a precision four-terminal shunt resistor or magnetic transducer. (Current through a solar cell should never be measured with a standard ammeter in series because the voltage bias developed across the meter will change the operating point of the cell.) Domestic and international standards have been developed for the minimum characteristics of typical $I-V$ measurement systems [5–7, 9, 11, 13]. The critical parameters on the $I-V$ curve are the open-circuit voltage (V_{OC}), the short-circuit current (I_{SC}), and the maximum-power point (P_{max}). Figure 16.8 shows a typical $I-V$ curve for a 50-W module in the light at SRC and in the dark. The fill factor (FF) is a normalized parameter indicating how ideal the diode properties are, and it is calculated by the following expression:

$$FF = \frac{P_{max}}{V_{OC} I_{SC}} \tag{16.32}$$

The fill factor is often expressed as a percentage by multiplying equation (16.32) by 100.

The open-circuit voltage can be determined from a linear fit to the $I-V$ curve around the zero current point or by measuring the voltage with the load disconnected. The value of V_{OC} is often obtained by linear interpolation of the two $I-V$ points closest to zero current. Performing a linear regression using more than two points can reduce the uncertainty in V_{OC}; however, care must be taken not to include points resulting from blocking diodes in series with a module or fitting in nonlinear regions. One manufacturer

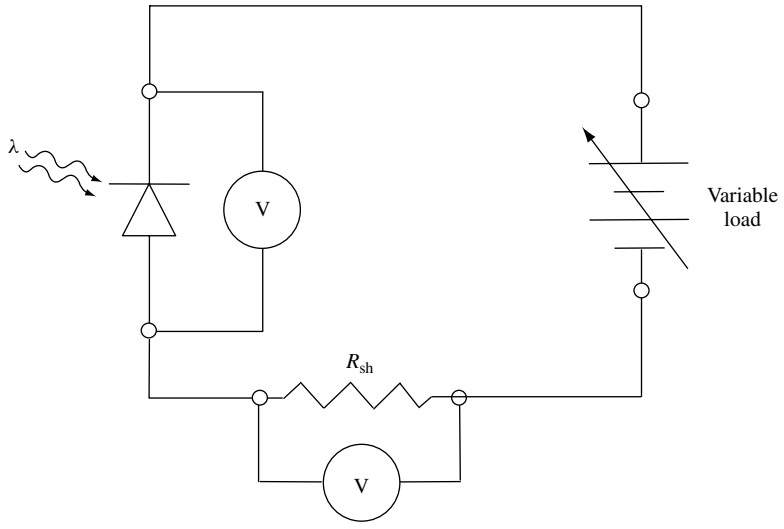

Figure 16.7 Typical current versus voltage measurement system

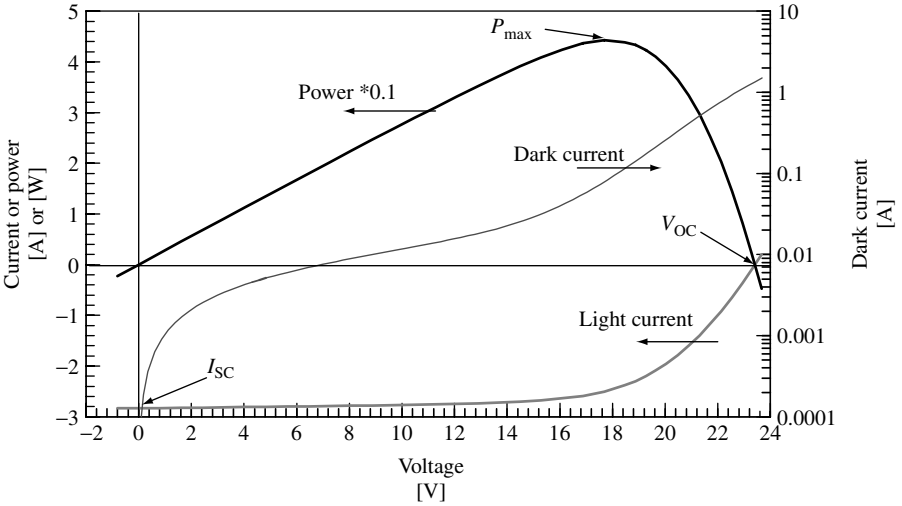

Figure 16.8 Typical light and dark current versus voltage curve of a commercial 50-W PV module

of commercial equipment includes the 20 $I-V$ points in the power quadrant closest to zero current. Another approach that works for all types of cells and modules is to include in the linear regression fit all points that satisfy the constraint that the absolute value of the voltage be less than 10% of the voltage at zero current and the additional constraint that the absolute value of the current be less than 20% of the current at zero voltage.

The value of I_{SC} is usually determined by linear interpolation of the two points closest to zero voltage. Performing a linear curve fit using more than two points can reduce the uncertainty in I_{SC}; however, care must be taken not to include points resulting from bypass diodes in parallel with a module or fitting in nonlinear regions. One manufacturer includes the 20 $I-V$ points in the power quadrant closest to zero voltage. Another approach that works for a wide variety of cells and modules is to include all $I-V$ points in the linear fit that satisfy the constraint that the current is within 4% of the current at zero voltage and the additional constraint that the absolute value of the voltage be less than 20% of the voltage at zero current. These constraints make no assumptions about the spacing between points (fit to a fixed number of $I-V$ points) or the shape of the curve (avoiding including nonlinear regions) while including as many $I-V$ points in the linear regression as possible.

The maximum power (P_{max}) is often taken to be the largest measured power. A more accurate method is to perform a fourth-order or higher polynomial curve fit to the measured power versus voltage data points within 80% of P_{max} [119]. To prevent erroneous results on low FF devices, the power versus voltage data selected for curve fitting must be restricted to voltages greater than 80% of the voltage at the measured maximum power (V_{max}). This algorithm can be improved by selecting the order of polynomial that gives the best fit to the data up to a fifth order. An approach recommended by American Society of Testing and Materials (ASTM) is to perform a fourth-order polynomial fit to the data where the measured current is greater $0.75I_{max}$ and less than $1.15I_{max}$ and

the measured voltage is greater than $0.75V_{max}$ and less than $1.15V_{max}$ [7]. The preceding constraints seem to work for cells and modules with a 40% fill factor to a 95% fill factor [119].

This allows the measured current to be corrected for intensity fluctuations to a constant intensity value. It is best to measure the incident irradiance with a reference cell at each current–voltage point and to use separate meters for the same sampling interval. A less accurate method is to measure the current and voltage sequentially with the same meter and only measure the intensity once. This method assumes that there are no temporal fluctuations in the simulated or natural light intensity during the measurement period and that the voltage is constant. This may not be the case if the bias rate or capacitance is large or if there are transients in the device [29, 119]. One commercial $I-V$ system averages 40 voltage readings and then 40 current readings to obtain a single $I-V$ point. This approach causes problems if the voltage and current are not in equilibrium because of too large a bias rate or other transient phenomena. A better approach would be to take 40 pairs of current and voltage points and then average the voltage and current because this relaxes the assumption that the current and voltage at a given load setting are random with time.

Useful additions that are rarely found in commercial $I-V$ equipment include checking for valid contacts and limiting the maximum current through the device. To prevent damage to PV cells, the resistance between the current and voltage contacts should be measured with manual or automatic measurements prior to the $I-V$ measurement. If the sample is too small for Kelvin contacts, then the current at zero voltage should be monitored while making contact with the cell. Most commercial systems are polarity-dependent because bipolar power supplies or loads are much more expensive. The current near zero volts is obtained by a low-voltage load of opposite polarity. This feature can damage cells and modules with a low reverse-bias breakdown such as amorphous silicon or GaAs if a diode is not placed in parallel with the sample to prevent a reverse-bias voltage from being applied. The polarity can easily be determined from the sign on the voltage near zero current or the sign on the current near zero voltage. This keeps the operator from worrying about which connection is positive and prevents excess bias voltages from accidentally being applied by automatically choosing a safe range for the maximum forward and reverse bias.

Commercial $I-V$ systems developed for the semiconductor industry by Hewlett Packard/Agilent Technologies Inc., Keithley Instruments Inc., and others are readily available. These units can be operated manually or with a computer with a wide range of features and capabilities including bipolar operation. The primary problem with units designed for transistor and diode analysis is the cost and limited maximum current. This limitation is only a problem for groups that need to perform $I-V$ measurements at biases over $\sim$100 V and $\sim$5 A. These generic $I-V$ systems require software to download the data, save it, and calculate relevant PV parameters. There is also a variety of manufacturers of PV test equipment for $I-V$ measurements including Daystar Inc., Spire Inc., Spectrolab Inc., Pasan Beval S.A., Wacom Electric Co. Ltd, and numerous other small companies. Commercial $I-V$ measurement software is typically designed for industrial applications and lacks the capability to detect bias rate artifacts by changing the bias direction, or variable bias, or load slew rate. Commercial software also has a fixed format for saving the data and plotting the results that may be difficult or impossible for the user to modify.

Most commercial $I-V$ software also measures only the light $I-V$ characteristics in the power quadrant. This is not sufficient for analyzing effects of nonohmic contacts requiring forward bias $I-V$ data beyond V_{OC} or voltage-dependent photocurrent collection requiring reverse bias $I-V$ data.

Many groups have developed custom data acquisition systems with commercial components. These systems are reviewed in Reference [2] and consist of electronics to measure the current and voltage and a power supply [1], operational amplifier [120, 121], capacitor [122], or transistors as the load [123–125]. Ideally, the current sense resistor should have a low temperature coefficient and have a power rating at least six times the maximum expected load power to prevent errors from changing ambient temperature or resistor heating. It should be noted that $I-V$ systems built around custom circuits and software could be difficult and time consuming to maintain when the developer is gone. In determining the most appropriate $I-V$ data acquisition system for devices that may range from single research-level cells to arrays, the present and all possible future applications should be considered. Any group that is considering building their first $I-V$ system, upgrading that old reliable $I-V$ system, or expanding their existing capabilities should consider the following factors:

- Desired outputs from the system – tabular and graphical display and hard copy of data, database or update of a simple directory text file, control over format and content of saved data, meteorological parameters.
- Minimum and maximum current and voltage range.
- Cost in time and money available for design and development.
- Cost in time and money available for maintenance (repairs, enhancements, and expansion).
- Compatibility with existing hardware, software, and databases.
- Flexibility to detect and compensate for artifacts – flexibility in bias direction and bias range, manual control, control over premeasurement illumination and bias state.

Assuming that the PV device is actually at SRC, the error in the FF is primarily affected by the connections to the data acquisition system. First and foremost, four-terminal (known as Kelvin) connections should always be used at the positive and negative terminals of the device. Between the point where positive or negative voltage connections are made and the PV sample, any wire or contact resistance will appear as a series resistance, reducing FF and hence P_{max} and η. At the component level of modules and above, wire resistance losses are included. For cells without wires attached, the goal is to simulate as accurately as possible the module-contacting scheme. This generally means placing a current and preferably a voltage probe contact at each wire bond pad. A temperature-controlled vacuum plate is used for compatible structures in which at least one of the positive or negative contacts is on the front surface (monocrystalline and multicrystalline wafers or thin-film devices deposited on a substrate) to provide a large-area, low-resistance contact. This low but finite contact resistance will appear as a power loss in P_{max} unless a separate voltage contact is used. This voltage contact may be a miniature, spring-loaded, blunt-tipped, gold-plated probe; a patterned, metallized Kapton or ceramic; a printed circuit board placed in a narrow slot in the vacuum plate; or some other method. The surface area of this voltage contact will introduce an error in the voltage when light is incident on the cell because of nonuniform heat transfer to the temperature-controlled

plate. For production PV testers, the ribbons attached to grids on Si cells are simulated by using linear arrays of probes (possibly spring-loaded to a specific force). At the cell level, many PV materials will be damaged if the probe penetrates the relatively thin contact pad or misses the pad and touches the semiconductor. When the contact geometries are small, a micromanipulator and microscope eyepiece may be required, and contacting problems tend to be more difficult. The typical probe contact procedure in the PV performance characterization laboratory at NREL is to choose the appropriately sized Kelvin probe mounted on a three-axis manipulator and make contact with the device, while monitoring the resistance between the voltage and current Kelvin contact. Kelvin probes are used with an attached coaxial cable manufactured by Accuprobe Inc., with CuBe tip diameters between 12.7 μm and 127 μm and contact spacing between 50.8 and 1524 μm. For large-area cells (10 cm by 10 cm or larger) designed to have ribbons attached, differences in fill factors of more than 50% between groups can occur [2, 126]. The source of these differences can be attributed to contacting and spatial nonuniformities in the light source. Contacting-related differences occur when probes are used to simulate the ribbons, because of variations in shadowing, and distributed resistance losses. Differences in I_{SC} of 2% between NREL and other groups have been attributed to light reflected off metal probe(s), nearby operators in white lab coats and fixturing. Custom-fixturing or optics to direct the light upward is often required when both contacts are on the side not being illuminated as is the case for point-contact or wrap-around Si cells, or for superstrate structures like a-Si or CdTe on transparent conducting oxide coated glass. Achieving temperature control and Kelvin-contacting for these structures is problematic. Groups have used patterned circuit boards or Kapton to achieve contacts and temperature control. The contact area is often the junction area for small area thin-film devices on insulating superstrates allowing a metal spool with a vacuum hold down to make thermal, and electrical contact to the metallized cell and a probe or wire to make contact to the transparent conducting oxide layer. Many of the best thin-film devices have a thick layer of In metal bonded to the transparent conducting oxide around the cell border to reduce lateral series resistance losses. High-efficiency research cells on insulating substrates such as Cu(Ga,In)(S,Se) also often have an In border around the cell area to reduce resistance losses.

Evaluating the performance of concentrator cells poses several challenges. As of 2001, there are no consensus standards to evaluate concentrator cells, although ASTM and the Commission for the European Community are developing standards. Issues of temperature measurement and control are aggravated by the large heat load. Typically, concentrator cells are evaluated under flash systems with a 1-ms pulse duration or under continuous illumination. If a continuous light source is used, then the temperature of the space charge region cannot be directly measured – any temperature sensor will affect the temperature because of the small thermal mass and large light level on the sample. There can be large differences in the temperature of the space charge region (i.e. the cell temperature) and the temperature of the vacuum plate or measured front-surface temperature. One approach with the cell in the dark or minimal heat load is to first set the temperature-controlled vacuum plate to a given temperature, and then measure V_{OC} as a function of time as a high-speed shutter is opened, exposing the sample to the full light level [127]. The V_{OC} will rise as the shutter is opened and the cell is exposed to the concentrated light and will go through a maximum as the cell heats up corresponding to the V_{OC} at the known temperature measured with no heat load. The plate temperature can then be reduced until this V_{OC} is obtained. The other primary problem

with concentrators is the measurement of E_{tot}. The simplest approach is to determine the one-sun I_{SC} and assume that this value is linear with light level. Another approach is to use calibrated neutral-density filters [2, 128, 129]. Neutral-density filters can be calibrated to better than 1% at a given wavelength using lasers, but typically they have a ±5% variation in transmissivity with wavelength over a 400- to 1100-nm range, limiting their usefulness to single-junction devices that are insensitive to spectral errors, such as Si and GaAs. The linearity can also be inferred by a series of measurements with aperture or changing flash-lamp voltage [111]. Other approaches to determining the linearity involve exposing the cell to low-level periodic sunlight and concentrated sunlight [130, 131]. Ideally, a calibrated linear reference cell should be used, but spatial nonuniformity of the concentrated beam can lead to a larger error than that if linearity had been assumed. Again, ideally, the spectral responsivity should be measured as a function of bias light level to address the issue that, for nonlinear devices, the spectral error M will change with total irradiance. Groups have developed spectral response systems capable of measuring the responsivity as a function of bias light level to about 200 suns [132, 133].

Concentrator modules cannot normally be measured in solar simulators because the optics are not a point source; the bulb(s) or integration optics will be imaged on the cell, resulting in a much larger spatial variation in intensity than that the module would encounter under natural sunlight. For this reason, concentrator modules are typically evaluated outdoors under natural sunlight over some period of time. There are no standards for concentrator cell, module or system measurements, although the PVUSA method in equation (16.2) has been used to evaluate concentrator systems [32, 43]. Concentrator modules and arrays evaluated at Sandia National Laboratories have consisted of the performance (P_{max}, or $I-V$ characteristics) as a function of direct-beam irradiance and heat sink temperature [129].

16.3.8 Solar Simulators

Solar simulators are used to simulate natural sunlight for repeatable and accurate indoor testing of the $I-V$ characteristics of PV cells or modules. The ideal solar simulator should have less than ±1% variation in the light level during the $I-V$ measurement period, less than a ±1% spatial variation in irradiance in and several cm above the test plane, and introduce less than a 1% spectral mismatch error between the test and reference cell. These constraints are essential to ensure an uncertainty in the efficiency of less than ±2%. Solar simulators are classified according to the spatial nonuniformity of the total irradiance, temporal instability of irradiance, total irradiance within a given field of view, and spectral match to the reference spectrum [134, 135]. Groups that evaluate multijunction cells and modules have found that single-source simulators can introduce large errors in I_{SC}, and P_{max}. Multisource solar simulators suitable for evaluating reference cells have been discussed in Section 16.3.6 [108–118, 136].

The temporal variation in light level during the $I-V$ measurement can be corrected if the intensity and device current are measured at the same time for each $I-V$ data point. Most commercial and custom $I-V$ systems for continuous light sources do not correct this temporal variation in the light level, although most groups have procedures in place to correct long-term drift in the simulator total irradiance over a period of hours or longer. The spatial uniformity varying with time for arc lamps cannot be readily

corrected, although placing the intensity monitor as close to the test device as possible can minimize these effects. A spatially nonuniform light source presents a measurement challenge of determining the average illumination level for a cell or the illumination level of the current-limiting cell in a module [126, 137]. The efficiency will always be reduced for nonuniform illumination compared to uniform illumination at the cell [138, 139] or module [140] level.

There are three types of illumination sources typically used for solar simulators: continuous arc, pulsed arc, and filament lamps. The merits and problems of these different simulators have been compared [28, 141–143]. If the distance between the test plane and the nearest optical surface is short, the possibility for reflection-related artifacts may exist [141]. These reflection-related artifacts occur because the field of view of the reference cell and test device are not identical and can occur from reflections off simulator optics, reference cell packages, probe fixtures, the test station enclosure, and the region underneath the test device. Light reflecting from the region under the test device is especially important for bifacial cells and superstrate structures.

With proprietary filters, commercial continuous Xe-arc lamp solar simulators have an excellent spectral match to the AM0 or terrestrial spectrum, and their point source (small arc volume) with integrating optics achieves a ± 1 to $\pm 3\%$ variation in spatial uniformity. The spectrum of these lamps shifts slightly from the blue to the red during the bulb life, with most of the spectral shift occurring in the first 100 h of operation [141]. The intensity of continuous arc lamps is controlled by changing the distance from the lamp to the test plane or by changing the current. Pulsed simulators are especially useful for characterizing concentrator cells and for large-area modules. The intensity of pulsed Xe-arc light sources is adjusted by changing the distance from the lamp to the test plane, by adjusting an aperture near the flash lamp, or by changing the voltage at which the lamp flashes. The spectrum of pulsed lamps shifts from the blue to the red less with the number of flashes of the lamp and is difficult to quantify because of the difficulty in measuring the spectral irradiance of pulsed light sources. The spectral match of unfiltered arc lamps in the UV and visible region is excellent but poor in the red (>700 nm) because of the numerous Xe emission lines. Custom filters reduce the magnitude of these lines to manageable levels. These emission lines are reduced for pulsed-Xe lamps.

The least expensive small-area light source is a tungsten-halogen lamp with a dichroic filter. These lamps are ideal for quantum efficiency measurements because of their irradiance temporal stability. The lamp spectrum depends strongly on the operating voltage or current [138]. A shift in the spectrum with bulb age has been attributed to tungsten-halogen lamps, but a careful study revealed that although the intensity drops with bulb age at a constant current, the shift with bulb age is less than the variation from bulb to bulb out of the same case [141]. To minimize spectral shifts of filament light sources with bulb age, they should be run at the same current throughout their life. The distance between the bulb and test plane should be varied to maintain the proper light level. There are a wide variety of tungsten-halogen bulbs with different wattage, lifetime, and voltage ratings. The choice of the most appropriate bulb is a compromise; for example, the ELH bulb has one of the highest wattages, but operates at 120 V and has a short lifetime of 35 h. Low-voltage bulbs such as the HLX, ELC, or HMM operate below 40 V, eliminating the safety hazard of higher voltage bulbs, and they have a longer life but a lower wattage. As with continuous arc lamps, the lamp lifetime is reduced by

frequently turning the lamp on and off. At least one module manufacturer uses an array of tungsten-halogen bulbs for production testing of modules in their multi-megawatt plant. They operate the bulbs at a low "simmer" voltage between $I-V$ measurements to greatly increase the lifetime of the bulbs. They use "matched" reference cells to minimize their sensitivity to spectral errors. The spectral irradiance of filament lamps is characterized by a black-body spectrum of 3200 to 3450 K. These lamps are deficient in the blue region of the solar spectrum because the AM0 spectrum can be approximated as a 5900 K black body.

16.4 SPECTRAL RESPONSIVITY MEASUREMENTS

The spectral responsivity ($S(\lambda)$) or quantum efficiency ($QE(\lambda)$) is essential for understanding current generation, recombination, and diffusion mechanisms in photovoltaic devices. PV cell and module calibrations often require a spectral correction factor that uses the spectral responsivity (i.e. equations 16.16–16.22). The spectral responsivity is measured in units of current produced per unit power and can be converted to quantum yield, or electron–hole pairs produced per incident photon through the equation:

$$QE(\lambda) = \frac{qS(\lambda)}{\lambda hc} \tag{16.33}$$

The factor hc/q equals 0.80655 for the wavelength in units of μm and the spectral responsivity in units of A/W. The quantum yield, in units of electron per photon, is often multiplied by 100, giving the quantum efficiency.

Typically, the spectral responsivity is measured at short-circuit current because it is easy to define and usually is the same as the photocurrent except for cells exhibiting voltage-dependent current collection like a-Si devices. PV devices normally operate near their maximum-power point. The spectral responsivity is assumed to be the same at the maximum-power and short-circuit points. Voltage-dependent spectral responsivities have been reported for a-Si [144], CdTe [145], and Cu(Ga,In)(S,Se) [146] material systems. (See Chapters 12, 13, and 14 for further discussion of voltage dependent collection in these types of devices).

The PV community has designed a variety of spectral response measurement systems, including ones based on interference filters, grating monochrometers, and interferometers [74, 77, 80, 81, 147–154]. For a single-junction solar cell, $S(\lambda)$ is determined by illuminating the cell with periodic (i.e. "chopped") monochromatic light and continuous broadband bias light of much greater intensity. The AC photocurrent from the device due to periodic monochromatic light is converted to an AC voltage and measured with a lock-in amplifier. An AC voltmeter may be used instead of a lock-in amplifier if the AC signal is large compared to the AC noise. The measured photocurrent is often in the μA to mA range with a broadband DC bias light near the device's intended operating point, for example, 1 sun.

For a two-terminal multijunction device, measuring the spectral responsivity of the individual junctions requires that the junction to be measured is the one which actually determines the photocurrent through the device (e.g. is the current-limiting junction).

Limiting the current is normally achieved by illuminating the other junctions *not* being measured with a DC bias light whose spectral irradiance covers their response range [154]. To measure $S(\lambda)$ for the *top* cell in a two-junction device, the bottom cell must be illuminated with "red" light that is absorbed mostly in the bottom cell. To measure $S(\lambda)$ for the *bottom* cell in a two-junction device, the top cell must be illuminated with "blue" light that is absorbed mostly in the top cell. In practice, the intensity of the bias light is increased until $S(\lambda)$ for the junction being measured is a maximum and $S(\lambda)$ values for the other junctions are minima. If the multijunction device terminals are at zero volts, then the cell being measured is at some reverse-bias voltage since the other junction is forward-biased owing to the bias light [154]. Because $S(\lambda)$ can depend on voltage, the cell being measured should be at zero volts, [154] which is accomplished by forward-biasing the multijunction cell. If each junction of a two-terminal device has about the same V_{OC}, then the cell should be forward-biased to half the V_{OC} of the tandem cell. In practice, the V_{OC} of the individual junctions is not well known; therefore, the forward-bias voltage must be adjusted to maximize the $S(\lambda)$ of the cell being measured and to minimize the $S(\lambda)$ of the other junctions. In practice, for an unknown multijunction device the procedure of increasing the bias light intensity and adjusting the bias voltage to maximize $S(\lambda)$ of the cell being measured while minimizing $S(\lambda)$ of the other junctions is an iterative process.

16.4.1 Filter-based Systems

A filter-based spectral responsivity $S(\lambda)$ measurement system is characterized by shining broadband light through interference filters and directing the light to the device under test, as shown in Figure 16.9 [147]. The filter wheel can be rotated with stepping solenoids controlled by digital logic or stepper motors. The use of the shutter shown in Figure 16.9 is essential when using an AC voltmeter to measure the signal when no monochromatic light is incident on the sample; it is less important though when using a lock-in amplifier to measure the periodic monochromatic signal. The monochromatic beam power is measured with a pyroelectric radiometer and calibrated Si detector. The reference detector can measure the power real time or the power versus wavelength data can be stored in a file. The advantage of real-time calibrations is that intensity fluctuations in the monochromatic beam can be corrected. The advantage of a stored calibration file is that the measured power is much higher, minimizing sensitivity to background light, and polarization effects associated with a beam splitter are not present.

It is often desirable to measure $S(\lambda)$ of modules consisting of multiple cells in series. The simplest approach would be to illuminate the whole module with AC monochromatic and AC broadband light with the module at 0 V, just as in the case of cells. Because of their high monochromatic light power density and large-beam area, filter-based $S(\lambda)$ systems are capable of fully illuminating any commercial module. The problem with this method is that different cells may be current limiting at various wavelengths, and the bias point of the current-limiting cell whose $S(\lambda)$ is being measured is not at 0 V. This problem is solved by voltage biasing, similar to the multijunction $S(\lambda)$ measurements [104, 154]. Figure 16.10 illustrates the geometry for measuring the spectral responsivity of an individual cell in a packaged module in which the individual cells are inaccessible.

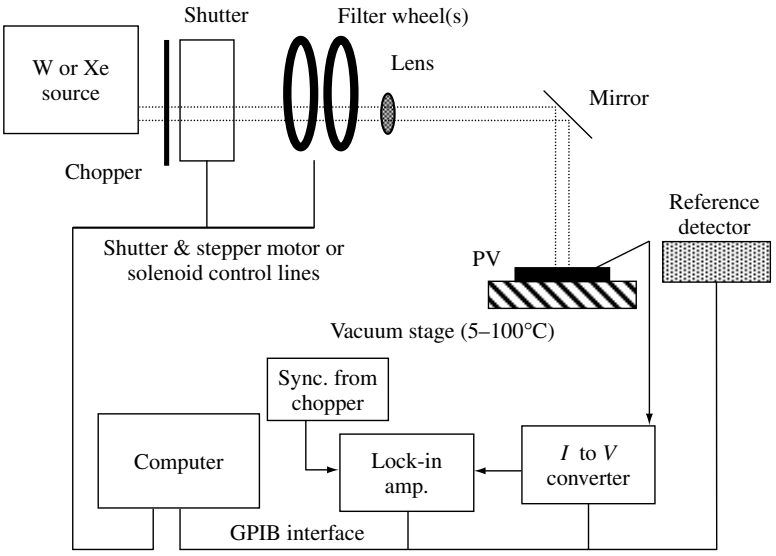

Figure 16.9 Typical narrow-band interference filter-based spectral responsivity measurement system

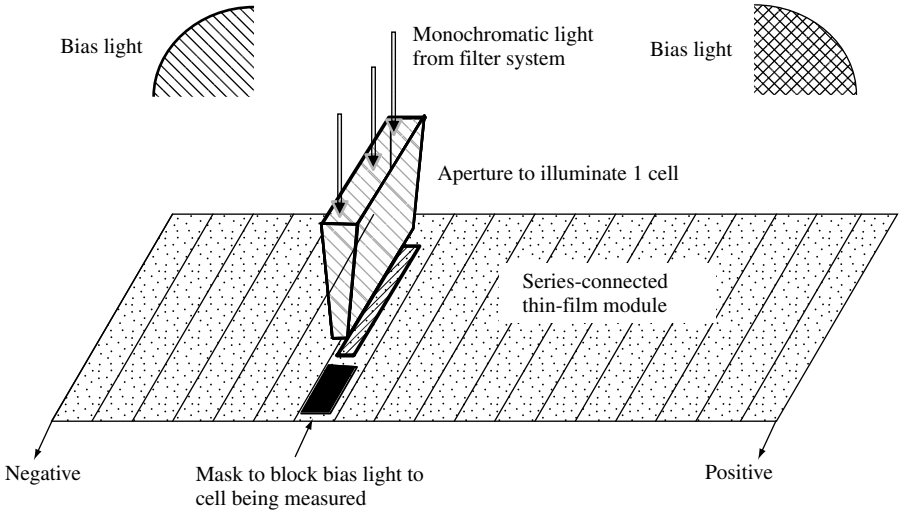

Figure 16.10 Apparatus for measuring the spectral responsivity of a single cell in a multicell module

The solution to the problem of measuring $S(\lambda)$ of a single cell in a module is the following sequence of steps [147]:

1. Bias the module with light to simulate "1 sun."
2. Forward-bias the module to the measured module open-circuit voltage (V_{OC}) under the bias light in the previous step multiplied by $(n-1)/n$, where n is the number of cells in series. Another procedure is to apply monochromatic light at a wavelength that the

cell responds to and then to reduce the forward-bias voltage from the measured V_{OC} toward 0 V until the AC signal is a maximum.

3. Shine the monochromatic light on only one cell.
4. By using a mask, reduce the bias light on the cell in step 3 in regions where there is no bias light. This procedure ensures that this cell is current limiting (see Figure 16.10).
5. Finally measure the $S(\lambda)$ of the chosen cell in the module.

If the cells $S(\lambda)$ in the module are not a function of bias light intensity, then the region where the monochromatic light illuminates the cell does not need to be illuminated by a DC bias light. To measure each junction in a multijunction module, the spectral content of the bias light must be adjusted and the voltage bias and intensity of the bias light must be iterated. These procedures have been shown to produce the same relative spectral responsivity for an electrically isolated cell in a module as when all of the cells in the module were series-connected [147].

16.4.2 Grating-based Systems

The grating system shown in Figure 16.11 was developed to measure the responsivity of cells from 400 to 3200 nm. Grating-monochrometer-based systems are especially useful for their broad-wavelength range and high spectral resolution. If a double-grating monochrometer is used, then the stray light in the UV can be eliminated, which is important for UV or high-bias-light measurements [77, 151]. Long wave pass order-sorting filters are commonly used to suppress modes (e.g. $\frac{1}{2}\lambda$) due to shorter wavelengths. For example, a Schott WG360 color glass filter is commonly used for $S(\lambda)$ measurements in the 400- to 700-nm region and a Schott RG630 filter is used as an order-sorting filter for measurements over a 700- to 1150-nm wavelength range. If a single-grating monochrometer is used with a tungsten light source, a band-pass filter may be needed for measurements

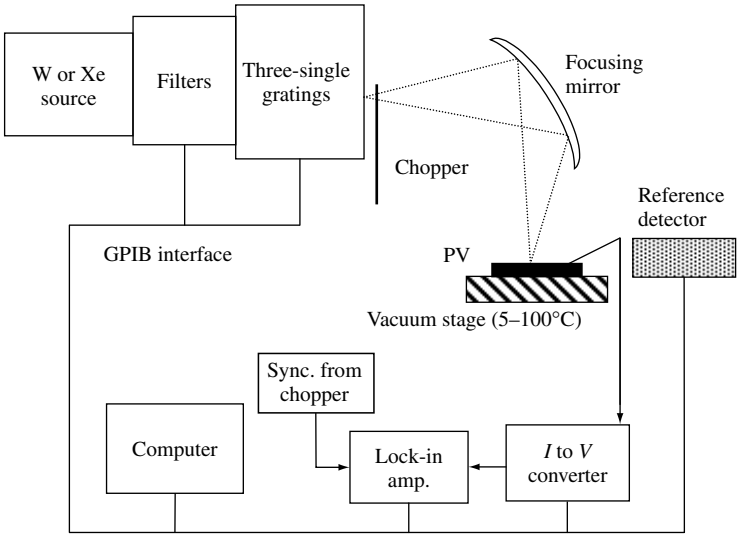

Figure 16.11 Typical grating-monochrometer-based spectral responsivity measurement system

in the 300- to 600-nm wavelength region to suppress modes at longer wavelengths and shorter wavelengths (e.g. $\frac{1}{2}\lambda$ and 2λ). The light power of the grating-monochrometer-based system can be focused on a rectangular spot of about 1 mm by 3 mm by imaging the monochrometer exit slits onto the test plane with a magnification of less than 1. Chromatic aberrations in the lens(es) cause the beam size to change with wavelength. This effect can be eliminated by eliminating all lenses and using a spherical or, better yet, a parabolic mirror. Typically, grating-based systems have lower optical throughput (lower intensity) but higher spectral resolution than filter-based systems.

16.4.3 Spectral Responsivity Measurement Uncertainty

Spectral responsivity measurements involve the measurement of the photocurrent produced by light of a given wavelength and power. The spectral responsivity is typically measured with bias light simulating reference conditions, because the device may be nonlinear [74, 77, 80, 81, 147–151, 154]. Typically, the spectral correction factor for efficiency measurements is calculated on the basis of $S(\lambda)$ measurements near 0 V and is assumed to be the same as at the maximum-power point. This assumption is valid for most PV systems and results in a negligible error for amorphous silicon, which has a voltage-dependent spectral responsivity [144, 155] assuming a reasonably well-matched reference cell is used such as a Schott KG5 filtered mono-Si cell.

The photocurrent is measured with a current-to-voltage converter. A power operational amplifier ($\pm$40 V, 8 A) with computer-controlled gain resistors (50 to 10 000 Ω) is useful for wide bias ranges and signal levels [147]. A simple current sense resistor may be adequate for systems that measure the same type of PV device all the time. The major limitation is that resistor and thermal noise at the microvolt level limits the measured currents to microamperes. Commercial current preamplifiers typically have a maximum current rating of 1 to 10 mA, limiting their usefulness for measuring the spectral responsivity with bias light (i.e. a 1 cm^2 device with $J_{SC} = 30\ mA\,cm^{-2}$ produces 30 mA of DC bias current with a 1 sun bias light). An operational amplifier configured as a current-to-voltage converter allows the insertion of a power supply in series with the PV device, giving a wide range of bias voltages. This feature is critical when measuring modules, multijunction devices, or devices with a voltage-dependent spectral responsivity [105, 147, 153]. Most groups use a lock-in amplifier to detect the periodic AC signal, but this is not required because the intense monochromatic light afforded with interference filters allows the AC signal to be amplified to the range where AC voltmeters are quite accurate [155]. Modern digital lock-in amplifiers have rapid auto-ranging capabilities and will outperform an AC voltmeter for noisy signals because of their large dynamic range. Error sources related to the measurement of the photocurrent are summarized in Table 16.7. If semiconductor-based calibrations are employed with the same electronics used to measure the test and reference device, then all multiplicative errors drop out. For pyroelectric-radiometer-based calibrations, the absolute photocurrent must be measured for absolute $S(\lambda)$ measurements.

For absolute current measurements, the measured lock-in signal must be multiplied by a waveform correction factor that relates the measured root-mean-square (RMS) signal

Table 16.7 Spectral responsivity error sources for measurement of the photocurrent

I. Electrical instrumentation
  A. Current-to-voltage (I to V) converter
    1. Commercial current amplifier, lock-in amplifier or custom amplifier gain, linearity, noise, offset, shunt resistor, calibration, drift, thermovoltages
  B. Signal from I to V converter measured with the following:
    1. Lock-in amplifier calibration, resolution, accuracy, waveform to sine wave correction factor, overloading, noise, dynamic range, time-constant, procedures for using lock-in amplifier
    2. An AC voltmeter gain, offset from noise level, linearity, time-constant
II. PV cell or module
  A. Temperature, response time to periodic light, linearity of PV device, white-light bias spatial uniformity, monochromatic light spatial uniformity, voltage bias of cell being measured, spectral content of bias light, device sensitivity to polarization of light
III. Mechanical
  A. Mechanical movement of optics, mechanical vibration, monochromatic beam wandering with wavelength, chopped stray monochromatic light

with the peak signal. This factor is $\sqrt{2}/2$ for a sine wave, $2\sqrt{2}$ for a square wave, and $2\sqrt{2}\ a\sin(\pi/a)/\pi^2$ for a trapezoid, with the constant π/a being the radian angle at the top of the rising edge of the trapezoidal waveform [156].

The response time of PV devices to chopped light can be a problem for electrochemical cells or those cells with many deep-level recombination centers. Many systems operate with chopping frequencies of 71–93 Hz as a compromise between stability, noise, and deep level response. Chopping frequencies below 4 Hz are required to keep the AC photoresponse independent of frequency [157]. This effect is more pronounced at low light levels and in the infrared. It is important that the light from the bias light source not be allowed to go through the light chopper. A simple procedure to determine if this artifact is present is to turn off the monochromatic light source and measure the test device's response as a function of bias light intensity.

Semiconductor-based calibrations are useful where the photocurrent is known within a multiplicative constant. Their primary limitation is their temperature sensitivity near the energy gap (wavelengths greater than 900 nm for Si) and their limited response range. Calibrated semiconductors are not commercially available for wavelength ranges beyond 300 to 1700 nm (Si-Ge hybrid detector). Accurate calibrations for semiconductor-based detectors are difficult to obtain for wavelengths greater than 1800 nm. If the same amplifier is used to measure the reference and unknown PV devices, then uncertainties in the gain drop out. For semiconductor calibrations, the chopper phase is irrelevant, whereas the electrically calibrated pyroelectric radiometer requires that the chopper be manually adjusted until the phase is correct. Semiconductor-based calibrations allow the test and reference signals to be filtered independently to maximize the signal-to-noise ratio. Various error sources associated with measuring the monochromatic light power are listed in Table 16.8. The measurement of the monochromatic light power can be performed with radiometric detectors or semiconductor detectors. When a quartz slide is used as the beam splitter, errors in the power can arise because of polarization effects. The light off the monochrometer is polarized, and the polarization angle can change with a grating change. The band gap, photoluminescence, and

Table 16.8 Spectral responsivity error sources for measurement of the light power

I. Filament or Xe-arc light source
   A. Intensity fluctuations, change in spectrum with age and current,
II. Real-time calibration
   A. Source-light polarization with a glass beam splitter, signal to noise, detector characteristics, calibration drift with time of monitor detector
III. Stored calibration file
   A. Monochromatic source calibration drift with time
IV. Stray light
   A. Detector sees light that cell does not see, area of detector different from device area, different field of views
   B. Monochrometer – incomplete attenuation of higher and lower grating orders, single versus double grating
   C. Narrow bandwidth filters – pinholes in the filter, degradation of blocking filter, insufficient blocking of light ($>10^{-4}$)
V. Detectors and associated electronics in general
   A. Calibration, resolution, accuracy, gain, phase, offset, linearity, spatial uniformity of detector element,
   B. Drift in temperature of room, change in the detector's field of view, degradation of detector,
   C. Spectral response of detector
VI. Pyroelectric detector
   A. Time constant of detector, microphonics, signal to noise, phase-angle adjustment, waveform factor (square wave assumed)

absorption coefficient for PV devices can be sensitive to the polarization angle. The light reflected from a glass surface will have a different polarization than the light reaching the test plane and will be of much lower intensity. These effects are minimized if a calibration is performed with the detector in the test plane and the file is stored to the disk. This procedure is required at least once for real-time calibrations. Real-time calibrations account for the change in spectrum with lamp age, current, and time.

If the beam is larger than the sample, then the spatial uniformity of the monochromatic beam is important. For the NREL filter monochrometer system, spatial nonuniformities of $\pm 10\%$ are typical and, more importantly, these errors can change with wavelength because of variations in the transmission of the filter and spatial variation in the output of the Xe-arc lamp. Electrically calibrated pyroelectric detectors are spectrally flat from the UV to far-infrared and have a low broadband error of less than $\pm 2\%$, but are sensitive to microphonics, temperature changes within the detector's field of view, and have noise at the 0.01 μWcm^{-2} level. Semiconductor-based detectors are not sensitive to light outside their relatively narrow response range and can be measured with the same electronics used to measure the test device, eliminating any wavelength-independent multiplicative error sources. Semiconductor-based detectors can drift with age [158] and have temperature coefficients exceeding $1\%/^{\circ}C$ near their band gap. Table 16.9 summarizes the error in the *QE* that can occur because of the monochromatic light. The bandwidth of the monochromatic light can contribute to the error near the band gap or when the light transmitted through a band-pass filter is highly asymmetric [156]. These errors have a small effect on the spectral correction factor when the full width at half-maximum bandwidth of the interference filters are less than 10 nm [156], as is commonly found in practice.

Table 16.9 Spectral responsivity error sources related to the monochromatic light

I.	Bandwidth, filter defects, polarization variation with wavelength
II.	Wavelength offset, wavelength error, wavelength variation with room temperature
III.	Beam wanders with wavelength
IV.	Beam larger than the test device
	A. Detector area versus PV area, position of detector and PV different, spatial uniformity of beam
V.	Beam smaller than detector and device area
	A. Partially shaded regions, spatial variation in responsivity of PV

16.5 MODULE QUALIFICATION AND CERTIFICATION

PV modules are designed to last 20 years or more in the field with no maintenance. Modules are designed to withstand daily thermal cycling, hail, wind, sand and storms, along with prolonged exposure to UV light. For safety reasons, PV cells and wiring must be isolated from the frame, edges, or module surface to prevent a hazardous electrical potential from forming. To verify that a particular product is reliable, domestic and international consensus standards have been developed for the design qualification and type approval of terrestrial crystalline silicon and thin-film modules [159–162].

Ideally, modules should be subjected to long-term exposure under natural conditions. Flat-plate silicon PV modules had poor reliability in the first years of development. An extensive program was conducted in the late 1970s and early 1980s by the JPL for the US government in an effort to improve the reliability of PV modules [163]. The 13 principal flat-plate module degradation mechanisms are open-circuited cell regions, shorted cells, open-circuited interconnects, gradual cell power degradation, optical degradation of the module package, front-surface soiling, glass breakage, open circuits in the module wiring, hot-spot failures of cells in a module, shorted bypass diodes, shorts to the frame or ground, delamination of the module encapsulant, and life-limiting wear out [163].

Accelerated testing procedures have been developed to simulate 20 or more years of exposure in the field and to identify the major failure mechanisms. Accelerated tests have been developed by various governmental organizations such as ASTM [161] or the Commission of European Communities [162, 164–166]. The tests described are from the International Electrotechnical Commission, the international standards organization relevant for photovoltaics [159, 163]. These tests include safety tests, mechanical integrity tests, and thermal cycling. The thermal-cycle test determines the ability of a module to withstand thermal expansion coefficient mismatch, fatigue, and other stresses caused by repeated changes in temperature, and it includes 200 thermal cycles from -40°C to $+85^{\circ}$C. The damp-heat test, designed to determine the module's ability to withstand the effects of long-term exposure to moisture in high-humidity environments, consists of 1000 h at 85% relative humidity at 85°C. The humidity-freeze test determines the ability of the module to withstand the effects of high temperature and humidity followed by subzero temperatures, and it consists of 10 cycles from 85% relative humidity and 85°C to -40°C. This is not a thermal-shock test because the maximum change in temperature with time above freezing temperatures is $100^{\circ}\text{C h}^{-1}$. This humidity-freeze test reveals the detrimental accumulation of liquid water inside the module under high-humidity

conditions. Because modules can have a substantially inferior performance under low light levels when they have a low shunt resistance, modules are tested at an irradiance of 200 Wm^{-2} (~only 20% of 1 sun). Modules exposed outdoors under short circuit conditions to 60 $kWh\,m^{-2}$ of total solar irradiation are required to sustain a loss in power of less than 5% to reveal any synergistic degradation effects that may not be detected by other tests. The hot-spot test is designed to ensure that modules will not fail when hot spots occur because of mismatched cells, partial shading, or interconnect failures. A hot spot is a localized region in a module that is operating at a significantly higher temperature (~5–40°C) than the rest of the module. The hot-spot test consists of five 1-h exposures at 1000 Wm^{-2} irradiance under the worst-case hot-spot condition. The modules must also survive a hail test of 25-mm-diameter ice balls directed at 11 impact locations with a velocity of 23 ms^{-1} [159, 163]. Modules are also subjected to a twist test to detect module defects that might arise when the module is mounted on a nonplanar surface. The twist test consists of supporting the module on three of its corners and deflecting the fourth corner 1.2° with respect to the plane defined by the other three corners [159, 160]. Modules are also expected to withstand wind, snow, or ice loads without mechanical or electrical failure. The static-load test simulates a wind load of 130 $km\,h^{-1}$, with a safety factor of 3, and consists of mounting the module in the manner prescribed by the manufacturer and applying a force of 2400 Pa uniformly to the front surface for 1 h and then the rear surface for 1 h. The insulation test is a safety test designed to determine if the current-carrying parts of the module are sufficiently well isolated from the module edges or frame and requires a resistance of greater than 50 MΩ at 500 V DC resistance to ground, and less than 50 μA current to ground at an applied voltage of 1000 V plus twice the maximum system voltage [159, 160]. For frameless modules, ground is obtained by attaching a metal conductor to the outside perimeter. The wet-leakage-current test is a stringent safety test to ensure that the current-carrying parts are well isolated, preventing a ground-fault condition from occurring even when the module is wet. The wet-leakage test is also designed to verify that moisture does not enter the active part of the module, where it might cause delamination or corrosion. The module is placed in a tank of water with resistivity of 3500 Ω-cm or less at 22°C ± 3°C and a surface tension less than 3 Nm^{-2} and the leakage current at 500 V is measured. The maximum allowed leakage current for the wet-leakage test (sometimes called the wet hi-pot test) is 10 μA plus 5 μA times the surface area in m^2. The wet-leakage test is performed before and after the various stress tests. The number of modules, sequence of events, and the pass/fail criteria are specified in the standard documents [156, 157]. Thin-film module testing procedures also require the $I-V$ characteristics under SRC to be measured periodically during light exposure (between 800–1000 Wm^{-2}, between 40–50°C) until the module power changes by less than 2% over 3 consecutive periods of at least 48 h [160, 166].

ACKNOWLEDGEMENTS

This work was supported in part under DOE Contract DE-AC36-99GO10337. The authors also wish to acknowledge the support of the National Center for Photovoltaics (www.nrel.gov/ncpv/) and the Measurements and Characterization Division (www.nrel.gov/measurements/). The assistance of D. Gwinner for editing is acknowledged.

REFERENCES

1. Emery K, Osterwald C, *Sol. Cells* **17**, 253–274 (1986).
2. Emery K, Osterwald C, *Current Topics in Photovoltaics*, Vol. 3, Chap. 4 Academic Press, London (1988).
3. Heidler K, Raicu A, Wilson H, *Proc. 21st IEEE Photovoltaic Specialist Conf.*, 1017–1022 (1990).
4. Nann S, Emery K, *Sol. Energy Mater.* **27**, 189–216 (1992).
5. Terrestrial Photovoltaic Measurement Procedures, NASA Tech. Report TM 73702 (June 1977).
6. Standard ASTM E948, *Standard Test Method for Electrical Performance of Non-Concentrator Photovoltaic Cells Using Reference Cells*, American Society for Testing and Materials, West Conshocken, PA, USA.
7. Standard ASTM E1036, *Standard Test Methods for Electrical Performance of Nonconcentrator Terrestrial Photovoltaic Modules and Arrays Using Reference Cells*, American Society for Testing and Materials, West Conshocken, PA, USA.
8. Standard ASTM E490-2000, *Standard for Solar Constant and Air Mass Zero Solar Spectral Irradiance Tables*, American Society for Testing and Materials, West Conshocken, PA, USA.
9. Standard Commission of the European Community, CEC 101, Issue 2, EUR-7078 EN, *Standard Procedures for Terrestrial Photovoltaic Measurements* (1981).
10. Standard ASTM E891-92, *Standard for Terrestrial Solar Direct Normal Solar Spectral Irradiance Tables for Air Mass 1.5*, American Society for Testing and Materials, West Conshocken, PA, USA.
11. Standard IEC 60904-1, *Photovoltaic Devices Part 1: Measurement of Photovoltaic Current-Voltage Characteristics*, International Electrotechnical Commission, Geneva, Switzerland.
12. Standard ASTM E892-92, *Standard for Terrestrial Solar Spectral Irradiance Tables at Air Mass 1.5 for a 37° Tilted Surface*, American Society for Testing and Materials, West Conshocken PA, USA.
13. Standard IEC 60904-3, *Measurement Principles for Terrestrial PV Solar Devices with Reference Spectral Irradiance Data*, International Electrotechnical Commission, Geneva, Switzerland.
14. Wehrli C, *Extraterrestrial Solar Spectrum*, Tech. Report 615, Physikalish-Meterologisches Observatorium and World Radiation Center, Davos-Dorf, Switzerland (July 1985).
15. ISO/DIS 15387, draft standard Space Systems – Single-Junction Space Solar Cells – Measurement and Calibration Procedures, International Organization for Standardization, Geneva, Switzerland.
16. *Solar Cell Array Design Handbook*, Tech. Report SP 43-38, Jet Propulsion Laboratory, Vol. 1, Pasadena, CA, USA (Oct. 1976).
17. Bird R, Hulstrom R, Riordan C, *Sol. Cells* **14**, 193–195 (1985).
18. Bird R, Hulstrom R, Lewis L, *Sol. Energy* **39**, 563–573 (1983).
19. Kurtz S *et al*., *Sol. Energy Mater. Sol. Cells* **62**, 379–391 (2000).
20. Myers D *et al*., *Proc. 28th IEEE Photovoltaic Specialist Conf.*, 1202–1205 (2000).
21. Osterwald C, *Proc. 18th IEEE Photovoltaic Specialist Conf.*, 951–956 (1985).
22. Emery K, Myers D, Kurtz S, *Proc. 29th IEEE Photovoltaic Specialist Conf.*, 840–843 (2002).
23. Faine P, Kurtz S, Riordan C, Olson J, *Sol. Cells* **312**, 259–278 (1991).
24. Standard ASTM Standard E490-73, *Standard for Solar Constant and Air Mass Zero Solar Spectral Irradiance Tables*, American Society for Testing and Materials, West Conshocken, PA, USA.
25. Makarova Y, Kharitonov A, *Distribution of Energy in the Solar Spectrum*, translated from Russian in NASA Tech. Report TT F-803 (June 1974).
26. Fröhlich C, Lean J, "Total Solar Irradiance Variations: The Construction of a Composite and its Comparison with Models", *Int. Astronomical Union Symp. 185: New Eyes to See Inside the Sun and Stars*, 89–102, Kluwer Academic Publishers, Dordrecht, The Netherlands (1998).

27. Standard ASTM E1328, *Standard Terminology Relating to Photovoltaic Solar Energy Conversion*, American Society for Testing and Materials, West Conshocken, PA, USA.
28. Emery K, *Sol. Cells* **18**, 251–260 (1986).
29. Emery K, Field H, *Proc. 24th IEEE Photovoltaic Specialist Conf.*, 1833–1838 (1994).
30. Green M *et al*., *Prog. Photovolt.* **9**, 49–56 (2001).
31. Firor K, *Proc. 18th IEEE Photovoltaic Specialist Conf.*, 1443–1448 (1985).
32. Jennings C, *Proc. 19th IEEE Photovoltaic Specialist Conf.*, 1257–1260 (1987).
33. Taylor R, *Sol. Cells* **18**, 335–344 (1986).
34. Fuentes M, *A Simplified Thermal Model for Flat-Plate Photovoltaic Arrays*, Sandia Tech. Report Sand 85–0330 (May 1987).
35. Koltay P, Wenk J, Bücher K, *Proc. 2nd World Conf. Photovoltaic Solar Energy Conversion*, 2334–2337 (1998).
36. Fisher H, Pschunder W, *Proc. 10th IEEE Photovoltaic Specialist Conf.*, 404–411 (1973).
37. DeWolf S *et al*., *Proc. 28th IEEE Photovoltaic Specialist Conf.*, 53–56 (2000).
38. Luft W *et al*., *Proc. 22nd IEEE Photovoltaic Specialist Conf.*, 1393–1398 (1991).
39. Luft W, von Roedern B, *Proc. 24th IEEE Photovoltaic Specialist Conf.*, 850–853 (1994).
40. DelCueto J, von Roedern B, *Prog. Photovolt.* **7**, 101–112 (1999).
41. Meyer T *et al*., *Proc. 26th IEEE Photovoltaic Specialist Conf.*, 371–374 (1997).
42. Ruberto M, Rothwarf A, *J. Appl. Phys.* **61**, 4662–4669 (1987).
43. Hester S, Townsend T, Clements W, Stolte W, *Proc. 21st IEEE Photovoltaic Specialist Conf.*, 937–943 (1990).
44. Gay C, Rumburg J, Wilson J, *Proc. 16th IEEE Photovoltaic Specialist Conf.*, 1041–1046 (1982).
45. Gianoli-Rossi E, Krebs K, *Proc. 8th Euro. Conf. Photovoltaic Solar Energy Conversion*, 509–514 (1988).
46. Kroposki B *et al*., *Proc. 25th IEEE Photovoltaic Specialist Conf.*, 1311–1314 (1996).
47. Kroposki B *et al*., *Proc. 28th IEEE Photovoltaic Specialist Conf.*, 1407–1411 (2000).
48. Whitaker C *et al*., *Proc. 26th IEEE Photovoltaic Specialist Conf.*, 1253–1256 (1997).
49. Marion B *et al*., *Validation of a Photovoltaic Module Energy Ratings Procedure at NREL*, NREL Tech. Report NREL/TP-520-26909 (Aug. 1999).
50. Marion W, Urban K, *User's Manual for TMY2s (Typical Meteorological Years) - Derived from the 1961–1990 National Solar Radiation Data Base*, NTIS/GPO Number: DE95004064, NREL Tech. Report TP-463-7688 (1995).
51. Nann S, Riordan C, *J. Appl. Met.* **30**, 447–462 (1991).
52. Raicu A, Heidler K, Kleiss G, Bücher K, *Proc. 11th Euro. Conf. Photovoltaic Solar Energy Conversion*, 1323–1326 (1992).
53. Raicu A, Heidler K, Kleiss G, Bücher K, *Proc. 22nd IEEE Photovoltaic Specialist Conf.*, 744–749 (1991).
54. Bücher K, *Proc. 23rd IEEE Photovoltaic Specialist Conf.*, 1056–1062 (1993).
55. King D, Dudley J, Boyson W, *Proc. 26th IEEE Photovoltaic Specialist Conf.*, 1295–1297 (1997).
56. Green M, *Solar Cells Operating Principles, Technology and System Application*, University of New South Wales, Kensington, Australia (1992).
57. Emery K *et al*., *Proc. 25th IEEE Photovoltaic Specialist Conf.*, 741–744 (1996).
58. Osterwald C, Glatfelter T, Burdick J, *Proc. 19th IEEE Photovoltaic Specialist Conf.*, 188–193 (1987).
59. Kameda M *et al*., *Proc. 25th IEEE Photovoltaic Specialist Conf.*, 1049–1052 (1996).
60. Hishikawa Y, Okamoto S, *Sol. Energy Mater. Sol. Cells* **33**, 157–168 (1994).
61. Sandstrom J, *A Method for Predicting Solar cell Current-Versus Voltage Characteristics as a Function of Solar Intensity and Cell Temperature*, JPL Tech. Report TR 32–1142, Jet Propulsion Laboratory, Pasadena, CA, USA (July 1967).

62. Standard IEC 60891, *Procedures for Temperature and Irradiance Corrections to Measured I-V Characteristics of Crystalline Silicon Photovoltaic Devices*, International Electrotechnical Commission, Geneva, Switzerland.
63. King D, Kratochvil J, Boyson W, Bower W, *Proc. 2nd World Conf. Photovoltaic Solar Energy Conversion*, 1947–1952 (1998).
64. Kasten F, Young A, *Appl. Opt.* **28**, 4735–4738 (1989).
65. Hishikawa Y, Imura Y, Oshiro T, *Proc. 28th IEEE*, 1464–1467 (2000).
66. Emery K *et al*., *Proc. 18th IEEE Photovoltaic Specialist Conf.*, 623–628 (1985).
67. Emery K, Osterwald C, *Sol. Cells* **27**, 445–453 (1989).
68. Field H, Emery K, *Proc. 23rd IEEE Photovoltaic Specialist Conf.*, 1180–1187 (1993).
69. Shimokawa R *et al*., *Sol. Cells* **19**, 59–72 (1987).
70. Emery K *et al*., *SERI Results from the PEP 1987 Summit Round Robin and a Comparison of Photovoltaic Calibration Methods*, NREL Tech. Report TR-213-3472 (March 1989).
71. Myers D, Emery K, Stoffel T, *Sol. Cells* **27**, 455–464 (1989).
72. Standard ASTM E1040, *Standard Specification for Physical Characteristics of Nonconcentrator Terrestrial Photovoltaic Reference Cells*, American Society for Testing and Materials, West Conshocken, PA, USA.
73. Standard IEC 60904-2, *Requirements for Reference Cells*, International Electrotechnical Commission, Geneva, Switzerland.
74. Osterwald C *et al*., *Proc. 26th IEEE Photovoltaic Specialist Conf.*, 1209–1212 (1997) also *Results of the PEP'93 Intercomparison of Reference Cell Calibrations and Newer Technology Performance Measurements: Final Report*, NREL Tech. Report NREL/TP-520-23477 (March 1998).
75. Osterwald C *et al*., *Prog. Photovolt.* **7**, 287–297 (1999).
76. Shimokawa R *et al*., *Jpn. J. Appl. Phys.* **28**, L845–L848 (1989).
77. Metzdorf J, *Appl. Opt.* **26**, 1701–1708 (1987).
78. Bruce S, *Optical Metrology and More*, NIST Tech. Report NISTIR 5429, U.S. Department of Commerce, National Institute of Standards and Technology, Gaithersburg, MD, USA (1994)
79. Allison J, Crab R, *Proc. 12th IEEE Photovoltaic Specialist Conf.*, 554–559 (1976).
80. Metzdorf J *et al*., *Proc. 21st IEEE Photovoltaic Specialist Conf.*, 952–959 (1990), also *The Results of the PEP '87 Round-Robin Calibration of Reference Cells and Modules – Final Report*, PTB Tech. Report PTB-Opt-31, ISBN 3-89429-06706, Braunschweig, Germany (Nov. 1990).
81. Ossenbrink H, Van Steenwinkel R, Krebs K, *The Results of the 1984/1985 Round-Robin Calibration of Reference Solar Cells for the Summit Working Group on Technology, Growth and Employment*, Tech. Report EUR 10613 EN, Joint Research Center, ISPRA Establishment, ISPRA, Italy (April 1986).
82. Osterwald C, *Sol. Cells* **18**, 269–279 (1986).
83. Osterwald C, Emery K, *J. Atmos. Oceanic Technol.* **17**, 1171–1188 (2000).
84. Romero J, Fox N, Fröhlich C, *Metrologia* **32**, 523–524 (1995/1996).
85. Gomez T, Garcia L, Martinez G, *Proc. 28th IEEE Photovoltaic Specialist Conf.*, 1332–1335, (2000).
86. Osterwald C, Emery K, Myers D, Hart R, *Proc. 21st IEEE Photovoltaic Specialist Conf.*, 1062–1067 (1990).
87. Shimokawa R *et al*., *Jpn. J. Appl. Phys.* **26**, 86–91 (1987).
88. King D, Hansen B, Jackson J, *Proc. 23rd IEEE Photovoltaic Specialist Conf.*, 1095–1101 (1993).
89. Bücher K *et al*., *Proc. 23rd IEEE Photovoltaic Specialist Conf.*, 1188–1193 (1993).
90. Anspaugh B, Downing R, Sidwell L, *Solar Cell Calibration Facility Validation of Balloon Flight Data: a Comparison of Shuttle and Balloon Flight Results*, JPL Tech. Report 85-78, Jet Propulsion Laboratory, Pasadena, CA, USA (1985).
91. Anspaugh B, *Proc. 19th IEEE Photovoltaic Specialist Conf.*, 542–547 (1987).

92. Brandhorst H, *Appl. Opt.* **4**, 716–718 (1968).
93. Brandhorst H, *Proc. International Colloquium Organized by ECOSEC*, 565–574 in *Solar Cells* (1971).
94. Bücher K, *Prog. Photovolt.* **5**, 91–107 (1997).
95. Emery K, Osterwald C, Kazmerski L, Hart R, *Proc. 8th Photovoltaic Solar Energy Conversion*, 64–68 (1988c).
96. Jenkins P, Brinker D, Scheiman D, *Proc. 26th IEEE Photovoltaic Specialist Conf.*, 857–860 (1997).
97. Standard ANSI/ASME PTC 19.1, *Part 1: Measurement Uncertainty*, American Society for Mechanical Engineers, New York, USA (1985).
98. Emery K, Osterwald C, *Sol. Cells* **27**, 445–453 (1989).
99. Emery K, Osterwald C, Wells C, *Proc. 19th IEEE Photovoltaic Specialist Conf.*, 153–159 (1987).
100. Whitfield K, Osterwald C, *Prog. Photovolt.* **9**, 87–102 (2001).
101. ISO Guide to the Expression of Uncertainty in Measurement, International Organization for Standardization, Geneva, Switzerland, ISBN 92-67-10199-9 (1993).
102. Emery K, *The Results of the First World Photovoltaic Scale Recalibration*, NREL Tech. Report NREL/TP-520-27942 (March 2000.)
103. Treble F, Krebs K, *Proc. 15th IEEE Photovoltaic Specialist Conf.*, 205–210 (1981).
104. Friedman D, *Proc. 25th IEEE Photovoltaic Specialist Conf.*, 89–92 (1996).
105. Virshup G *et al*., *Proc. 21st IEEE Photovoltaic Specialist Conf.*, 336–338 (1990).
106. Matsuda S, Flood D, Gomez T, Yiqiang Y, *Proc. 2nd World Conf. Photovoltaic Solar Energy Conversion*, 3572–3577 (1988).
107. Bogus K, Larue J, Masson J, Robben A, *Proc. 6th Euro. Conf. Photovoltaic Solar Energy Conversion*, 348–354 (1985).
108. Glatfelter T, Burdick J, Czubatyj W, *Proc. 2nd Photovoltaic Solar Energy Conversion*, 106–109 (1986).
109. Glatfelter T, Burdick J, *Proc. 19th IEEE Photovoltaic Specialist Conf.*, 1187–1193 (1987).
110. Virshup G, *Proc. 21st IEEE Photovoltaic Specialist Conf.*, 1249–1255 (1990).
111. Emery K *et al*., *Proc. 28th IEEE Photovoltaic Specialist Conf.*, 1126–1130 (2000).
112. Bickler D, *Sol. Energy* **6**, 64–68 (1962).
113. Bennett M, Podlesny R, *Proc. 21st IEEE Photovoltaic Specialist Conf.*, 1438–1442 (1990).
114. Shimokawa R, Nagamine F, Hamyashi Y, *Jpn. J. Appl. Phys.* **25**, L165–L167 (1986).
115. Sopori B, Marshall C, Emery K, *Proc. 21st IEEE Photovoltaic Specialist Conf.*, 1116–1121 (1990).
116. Sopori B, Marshall C, *Proc. 22nd IEEE Photovoltaic Specialist Conf.* (1991).
117. Adelhelm R, Bücher K, *Sol. Energy Mater. Sol. Cells* **50**, 185–195 (1998).
118. Muesel M *et al*., *Prog. in Photovolt.* **10**, 243–255 (2001).
119. Emery K, Osterwald C, *Proc. 21st IEEE Photovoltaic Specialist Conf.*, 1068–1073 (1990).
120. Schultz P, Meilus A, Hu S, Goradia C, *IEEE Trans. Inst. Meas.* **IM26**, 295–299 (1977).
121. Briskman R, Livingstone P, *Sol. Energy Mater. Sol. Cells* **46**, 187–199 (1997).
122. Cox C, Warner T, *Proc. 16th IEEE Photovoltaic Specialist Conf.*, 277–1283 (1982).
123. Skolnik H, *Sol. Energy* **14**, 43–54 (1972).
124. Kern R, Wagemann W, *Proc. 7th Euro. Conf. Photovoltaic Solar Energy Conversion*, 314–318 (1986).
125. Mantingh E, Zaaiman W, Ossenbrink H, *Proc. 24th IEEE Photovoltaic Specialist Conf.*, 871–873, (1994).
126. Heidler K, Fischer H, Kunzelmann S, *Proc. 9th Euro. Conf. Photovoltaic Solar Energy Conversion*, 791–794 (1989).
127. Moriarty T, Emery K, *Proc. 4th NREL TPV Conf.*, AIP Proceedings Vol. 460, 301–311 (1998).
128. Gee J, Hansen R, *Sol. Cells* **18**, 281–286 (1986).
129. Nasby R, Sanderson R, *Sol. Cells* **6**, 39–47 (1982).

130. Dondero R, Zirkle T, Backus C, *Proc. 18th IEEE Photovoltaic Specialist Conf.*, 1754–1755 (1985).
131. Martin S, Backus C, *Proc. 6th Euro. Conf. Photovoltaic Solar Energy Conversion*, 290–294 (1985).
132. Chambers B, Backus C, *Proc. 3rd Euro. Conf. Photovoltaic Solar Energy Conversion*, 418–422 (1980).
133. Stryi-Hipp G *et al.*, *Proc. 23rd IEEE Photovoltaic Specialist Conf.*, 303–308 (1993).
134. Standard ASTM E927, *Standard Specification for Solar Simulation for Terrestrial Photovoltaic Testing*, American Society for Testing and Materials, West Conshocken, PA, USA.
135. Standard International Electrotechnical Commission IEC 60904-9, *Solar Simulator Performance Requirements*, Geneva, Switzerland.
136. Krut D, Lovelady J, Cavicchi T, *Proc. 2nd World Conf. Photovoltaic Solar Energy Conversion*, 3671–3674 (1998).
137. Cuevas A, Lopez-Romero S, *Sol. Cells* **11**, 163–173 (1984).
138. Dhariwal S, Mathur R, Gadre R, *J. Phys. D: Appl. Phys.* **14**, 1325–1329 (1981).
139. Schönecker A, Bücher K, *Proc. 22nd IEEE Photovoltaic Specialist Conf.*, 203–208 (1991).
140. King D, Dudley J, Boyson W, *Proc. 25th IEEE Photovoltaic Specialist Conf.*, 1295–1297, (1996).
141. Emery K, Myers D, Rummel S, *Proc. 20th IEEE Photovoltaic Specialist Conf.*, 1087–1091 (1989).
142. Seaman C, Anspaugh B, Downing R, Esty R, *Proc. 14th IEEE Photovoltaic Specialist Conf.*, 494–499 (1980).
143. Matson R, Emery K, Bird R, *Sol. Cells* **11**, 105–145 (1984).
144. Hegedus S, *Prog. Photovolt.* **5**, 151–168 (1997).
145. Fardig D, Phillips J, *Proc. 22nd IEEE Photovoltaic Specialist Conf.*, 1146–1150 (1991).
146. Shafarman W, Klenk R, McCandless B, *J. Appl. Physics* **79**, 7324–7328 (1996).
147. Emery K, Dunlavy D, Field H, Moriarty T, *Proc. 2nd World Conf. Photovoltaic Solar Energy Conversion*, 2298–2301 (1998).
148. Standard ASTM E1021, *Standard Test Methods for Measuring Spectral Response of Photovoltaic Cells*, American Society for Testing and Materials, West Conshocken, PA, USA.
149. Bücher K, Schönecker A, *Proc. 10th Euro. Conf. Photovoltaic Solar Energy Conversion*, 107–110 (1991).
150. Hartman J, Lind M, *Sol. Cells* **7**, 147–157 (1982).
151. Stryi-Hipp G *et al.*, *Proc. 23rd IEEE Photovoltaic Specialist Conf.*, 303–308 (1993).
152. Jing-Gui C, Xiong-Jun G, Pei-Neo Y, Yu-Xue W, *Proc. 3rd Photovoltaic Solar Energy Conversion*, 743–748 (1987).
153. Schill C, Bücher K, Zastrow A, *Proc. 14th Euro. Conf. Photovoltaic Solar Energy Conversion*, 309–312 (1997).
154. Burdick J, Glatfelter T, *Sol. Cells* **18**, 301–314 (1986).
155. Shafarman W, Klenk R, McCandless B, *J. Appl. Phys.* **79**, 7324–7328 (1996).
156. Field H, *Proc. 26th IEEE Photovoltaic Specialist Conf.*, 471–474 (1997).
157. Sommeling P *et al.*, *Proc. 14th Euro. Conf. Photovoltaic Solar Energy Conversion*, 1816–1819 (1997).
158. Stock K, Heine R, *Optik* **71**, 137–142 (1985).
159. International Electrotechnical Standard Commission IEC 61215, *Crystalline Silicon Terrestrial Photovoltaic (PV) Modules – Design Qualification and Type Approval*, Geneva, Switzerland.
160. International Electrotechnical Commission Standard IEC 61646, *Thin-Film Terrestrial Photovoltaic (PV) Modules – Design Qualification and Type Approval*, Geneva, Switzerland.
161. Osterwald C, "ASTM Standards Development Status", *Proc. 18th IEEE Photovoltaic Specialist Conf.*, 749–753 (1985).
162. *Qualification Test Procedures for Photovoltaic Modules*, Commission of the European Communities, Joint Research Center, ISPRA Establishment, Specification 502 (May 1984).

163. Ross R, *Proc. 17th IEEE Photovoltaic Specialist Conf.*, 464–472 (1984).
164. Krebs K *et al.*, *Proc. 5th Euro. Conf. Photovoltaic Solar Energy Conversion*, 597–603 (1983).
165. Dunlop E, Bishop J, Ossenbrink H, *Proc. 2nd World Conf. Photovoltaic Solar Energy Conversion*, 459–462 (1998).
166. Bishop J, Ossenbrink H, *Proc. 25th IEEE Photovoltaic Specialist Conf.*, 1191–1196 (1996).